Atmos. Chem. Phys. Discuss., 13, 25013–25065, 2013
www.atmos-chem-phys-discuss.net/13/25013/2013/
doi:10.5194/acpd-13-25013-2013

Atmospheric Chemistry and Physics Discussions

AERONET-based microphysical and optical properties of smoke-dominated aerosol near source regions and transported over oceans, and implications for satellite retrievals of aerosol optical depth

A. M. Sayer[1,2], **N. C. Hsu**[1], **T. F. Eck**[1,2], **A. Smirnov**[1,3], **and B. N. Holben**[1]

[1]NASA Goddard Space Flight Center, Greenbelt, Maryland, USA
[2]Goddard Earth Sciences Technology And Research (GESTAR), Universities Space Research Association (USRA), Columbia, Maryland, USA
[3]Sigma Space Corporation, Lanham, Maryland, USA

Received: 5 August 2013 – Accepted: 27 August 2013 – Published: 25 September 2013

Correspondence to: A. M. Sayer (andrew.sayer@nasa.gov)

Published by Copernicus Publications on behalf of the European Geosciences Union.

Abstract

Smoke aerosols from biomass burning are an important component of the global aerosol cycle. Analysis of Aerosol Robotic Network (AERONET) retrievals of size distribution and refractive index reveals variety between biomass burning aerosols in different global source regions, in terms of aerosol particle size and single scatter albedo (SSA). Case studies of smoke transported to coastal/island AERONET sites also mostly lie within the range of variability at near-source sites. Two broad 'families' of aerosol properties are found, corresponding to sites dominated by boreal forest burning (larger, broader fine mode, with midvisible SSA ~0.95), and those influenced by grass, shrub, or crop burning with additional forest contributions (smaller, narrower particles with SSA ~0.88–0.9 in the midvisible). The strongest absorption is seen in southern African savannah at Mongu (Zambia), with average SSA ~0.85 in the midvisible. These can serve as candidate sets of aerosol microphysical/optical properties for use in satellite aerosol optical depth (AOD) retrieval algorithms. The models presently adopted by these algorithms over ocean are often insufficiently absorbing to represent these biomass burning aerosols. A corollary of this is an underestimate of AOD in smoke outflow regions, which has important consequences for applications of these satellite datasets.

1 Introduction

For several decades, satellite observations have provided a powerful tool for monitoring many aspects of the Earth system, including the atmospheric aerosol loading. Quantities such as aerosol optical depth (AOD) have generally been retrieved with lower uncertainties over oceans than land surfaces, due to the comparative homogeneity of open ocean surface properties and general lack of strong oceanic aerosol point sources. Despite this, significant differences can still exist between AOD retrieved using different instruments or algorithms, in both clean and polluted conditions, and for

ACPD
13, 25013–25065, 2013

real measurements as well as simulated data (Remer et al., 2008; Kokhanovsky et al., 2010; Sayer et al., 2012a).

To some extent, these differences can be the result of differences between sensor radiometric calibration, cloud screening, or sampling-related issues such as pixel/retrieval weighting and averaging techniques (Mishchenko et al., 1999; Kaufman et al., 2005; Kahn et al., 2007; Levy et al., 2009; Sayer et al., 2010b). However, even over oceans, measurements made by past and current passive satellite sensors generally do not provide sufficient information to retrieve unambiguously all relevant parameters of interest, such as spectral and directional surface reflectance, and aerosol microphysical properties and vertical distribution (Hasekamp and Landgraf, 2005). Thus, algorithms must make assumptions about these quantities, tied to the particular strengths and weaknesses of the instrument in question. Specifically, most algorithms parametrise oceanic surface reflectance as a combination of wind-roughened Sun-glint and foam, with an additional contribution linked to oceanic chlorophyll concentration (e.g. Sayer et al., 2010a). Additionally, aerosols are often assumed to consist of a mixture of components whose total abundance and relative weight are varied in order to best match the top-of-atmosphere (TOA) radiance observed by the sensor (e.g. Martonchik et al., 1998; Mishchenko et al., 1999; Remer et al., 2009; Thomas et al., 2009; Sayer et al., 2012a). These algorithmic assumptions also contribute to uncertainty in retrieved aerosol properties, and the disparity between available satellite-derived datasets.

As the AOD increases, so does its contribution to the TOA signal in the shortwave (and in some cases longwave) spectrum, and so the sensitivity of the retrieval algorithm to these assumptions about aerosol composition (e.g. Bulgin et al., 2011; Lee et al., 2012). It is therefore important that these assumptions are realistic, in order to minimise errors in retrieved AOD. Existing datasets typically use microphysical properties derived from in-situ measurements, semi-empirical considerations, or else leverage retrievals of microphysical properties from sources with a higher information content, such as those in the Aerosol Robotic Network (AERONET; Holben et al., 1998). An exception to this is the Polarization and Directionality of the Earth's Reflectance (POLDER)

ACPD
13, 25013–25065, 2013

sensor, whose multidirectional and polarisation measurements offer an increased information content, allowing algorithms to use weaker constraints about microphysical assumptions as compared to other sensors (Dubovik et al., 2011; Hasekamp et al., 2011).

Aerosol over the ocean is typically composed of a combination of hydrated sea salt particles and biogenic organic aerosols (O'Dowd and de Leeuw, 2007), with (regionally- and seasonally-dependent) contributions from transported continental aerosols (such as sulphates, nitrates, carbonaceous aerosols from industry or biomass burning, and mineral dust). Sayer et al. (2012b) present an AERONET-derived model for unpolluted and dust-free marine aerosol. Microphysical properties of mineral dust (McConnell et al., 2008; Ansmann et al., 2011; Su and Toon, 2011; Lee et al., 2012; Ryder et al., 2013) and continental/industrial pollution (Dubovik et al., 2002; Aiken et al., 2009; Giles et al., 2011, 2012; McMeeking et al., 2011) have been well-studied using both AERONET data and field campaigns or monitoring sites. The focus of this study is to examine the microphysical properties of smoke-dominated aerosol mixtures transported to oceanic regions, and compare these to the properties of smoke nearer to source regions.

Biomass burning is an important part of the global aerosol burden. Smoke aerosols near their source regions are strongly optically-dominated by fine-mode absorbing particles, with properties dependent on the substance which is burning as well as type of combustion (flaming vs. smouldering) and temperature/moisture content (e.g. regional/global reviews by Streets et al., 2003; Reid et al., 2005a, b; Janhäll et al., 2010). Comparatively less well-studied are properties after medium- and long-range transport to the oceans, where processes such as chemical ageing, wet/dry deposition, and mixing with air masses of different origins may alter the microphysical properties of the columnar aerosol. Note, however, that some chemical changes within the aerosol occur fairly rapidly after emission (such as coagulation and moisture uptake), so even for near-source sites time differences of order of an hour or less can mean aerosol

ACPD
13, 25013–25065, 2013

microphysical and radiative properties differ from those at the time of emission (Radke et al., 1991; Hobbs et al., 1997; Martins et al., 1997; Magi and Hobbs, 2003).

The analysis herein proceeds as follows. Section 2 discusses the AERONET data and assorted notation used. Then, the microphysical properties of smoke aerosols from AERONET sites near major global biomass burning source regions are examined in Sect. 3. As there are limited in situ measurements or AERONET sites located in the common biomass burning oceanic outflow regions, these climatological properties are then compared to cases of occasional smoke transport to coastal/island AERONET sites in Sect. 4. Section 5 illustrates potential biases in existing over-ocean satellite AOD datasets as a result of insufficient absorption in presently-assumed aerosol microphysical properties, and Sect. 6 provides a perspective on the importance of the results.

2 AERONET data

The sun photometers used by AERONET measure spectral direct-beam solar radiance, as well as directional diffuse radiance in the solar almucantar. The former are used to determine columnar spectral AOD and water vapour, provided at a temporal resolution of approximately 10–15 min. Throughout this study, the AOD is denoted τ_λ where λ is the wavelength in nm. AERONET direct-Sun AOD has a typical uncertainty of 0.01–0.02 (Holben et al., 1998; Eck et al., 1999) and is provided at multiple wavelengths (dependent on site) between 340 nm and 1640 nm. The Ångström exponent, $\alpha = -d\ln\tau / d\ln\lambda$, is also derived by AERONET; references to α herein indicate that calculated over the wavelength range 440 nm–870 nm (by regression of all available τ_λ over that wavelength range).

The spectral AOD is also used, along with almucantar measurements of sky radiance taken over a large range of scattering angles, in the inversion algorithm of Dubovik and King (2000), Dubovik et al. (2006). This retrieves aerosol volume size distribution (in 22 logarithmically-spaced bins with radii r from 0.05 µm-15 µm) and spectral complex

ACPD
13, 25013–25065, 2013

refractive index at 440 nm, 675 nm, 870 nm, and 1020 nm. Cloud screening and other quality checks (Smirnov et al., 2000, Holben et al., 2006) are performed in order to remove potentially unreliable retrievals. Retrievals passing these checks are denoted "level 2"; for biomass burning aerosols and moderate aerosol loadings ($\tau_{440} \sim 0.4$), associated uncertainties for such retrievals are 25 % on the binned size distribution (for $0.1\,\mu\text{m} < r < 7\,\mu\text{m}$, and larger on the tails), 0.04 on the real part of the refractive index, and 30 % on the imaginary part of the refractive index, giving an uncertainty in aerosol single scattering albedo (SSA, denoted ω_0) of approximately 0.03 (Dubovik et al., 2000). Higher AOD can decrease some of these uncertainties further. Size distributions remain reliable at lower aerosol loadings, although refractive index uncertainties increase significantly.

The notation adopted herein for aerosol microphysical properties follows that of Sayer et al. (2012b) and numerous other AERONET-based studies. The number size distribution $dN(r)/d\ln(r)$ describes the number of aerosol particles with radius in the infinitesimal size range $r \pm d\ln(r)$; the related volume size distribution is

$$\frac{dV(r)}{d\ln(r)} = \frac{4\pi r^3}{3}\frac{dN(r)}{d\ln(r)}, \tag{1}$$

for spherical particles. Total columnar aerosol particle number (C_n) and volume (C_v) are obtained by integrating these distributions over $\ln(r)$. The logarithmic volume mean radius (r_v) is a frequently-used metric of average aerosol particle size, defined

$$\ln(r_v) = \frac{\int_{-\infty}^{\infty} \ln(r)\frac{dV(r)}{d\ln(r)}d\ln(r)}{\int_{-\infty}^{\infty} \frac{dV(r)}{d\ln(r)}d\ln(r)}; \tag{2}$$

ACPD
13, 25013–25065, 2013

also often-used is the effective radius (r_{eff}), which is the ratio of the third to the second moment of the size distribution. The broadness of the distribution is often characterised by its spread (also called width), σ, where

$$\sigma = \sqrt{\frac{\int_{-\infty}^{\infty} (\ln(r) - \ln(r_{\mathrm{v}}))^2 \frac{dV(r)}{d\ln(r)} d\ln(r)}{\int_{-\infty}^{\infty} \frac{dV(r)}{d\ln(r)} d\ln(r)}}. \quad (3)$$

The geometric standard deviation, e^{σ} in this notation, is sometimes used instead of σ. The above definitions are independent of the shape of the size distribution. In practice, aerosol size distributions are often represented as a combination of lognormally-distributed components (because real size distributions often closely follow a lognormal distribution, as well as for the mathematical/computational conveniences afforded by these distributions). In this case, the number size distribution is defined as a summation over n_{c} components by

$$\frac{dN(r)}{d\ln(r)} = \sum_{i=1}^{n_{\mathrm{c}}} \frac{C_{\mathrm{n},i}}{\sqrt{2\pi}\sigma_i} e^{-\frac{1}{2}\left(\frac{\ln(r) - \ln(r_{\mathrm{n},i})}{\sigma_i}\right)^2}, \quad (4)$$

and the modal radius for each component is also its median and geometric mean. The equivalent formulation for aerosol volume is arrived at by substituting r_{n} with r_{v}, and C_{n} with C_{v}. For a lognormal component, conversions between number and volume quantities are (Sayer et al., 2012b)

$$r_{\mathrm{v}} = r_{\mathrm{n}} e^{3\sigma^2}, \quad (5)$$

$$C_{\mathrm{v}} = \frac{4\pi}{3} {r_{\mathrm{n}}}^3 e^{4.5\sigma^2} C_{\mathrm{n}}, \quad (6)$$

ACPD
13, 25013–25065, 2013

and additionally

$$r_{\text{eff}} = r_{\text{n}} e^{2.5\sigma^2} = r_{\text{v}} e^{-0.5\sigma^2}. \quad (7)$$

Observed aerosol size distributions are typically (although not exclusively) bimodal ($n_{\text{c}} = 2$), e.g. Dubovik et al. (2002). In these cases, and adopted here, the smaller (fine) mode properties are denoted with a subscripted f (i.e. $r_{\text{v,f}}$, σ_{f}) and the larger (coarse) mode properties with a subscripted c. Analagously, fine and coarse mode AOD are denoted $\tau_{\text{f},\lambda}$ and $\tau_{\text{c},\lambda}$ respectively. This AERONET dataset defines fine and coarse mode properties by locating the inflection point in the retrieved size distribution; as the distributions studied in this work consist of two distinct peaks, results are numerically only weakly sensitive to the precise fine/coarse demarcation point (coarse mode more so than fine, when τ_{c} is low).

Propagating the aforementioned errors on retrieved aerosol size distribution (Dubovik et al., 2000) onto these distribution parameters (for a typical biomass burning model from Dubovik et al., 2002, and assuming errors in each bin of $dV(r)/d\ln(r)$ are uncorrelated) suggest uncertainties on AERONET-derived $r_{\text{v,f}}$ of 0.01 µm, σ_{f} of 0.06, $r_{\text{v},c}$ of 0.2 µm, and σ_{c} of 0.06 for individual retrievals. Throughout this work, "fine" refers to accumulation-mode aerosols; smaller "nucleation-mode" aerosols may also be present, with some of these existing on the smaller-r tail of the fine mode, and others below this limit (although in that case so small as to be optically inactive in this spectral range). Mie theory is used throughout; although fresh smoke particles may be nonspherical, they rapidly coagulate to form aggregates whose radiative properties (in contrast to nonspherical coarse aerosols such as mineral dust) have been found to be modelled adequately by Mie theory (Kahn et al., 1997; Mishchenko et al., 1997; Reid and Hobbs, 1998; Dubovik et al., 2000, 2006; Reid et al., 2005b).

ACPD
13, 25013–25065, 2013

3 Properties of smoke aerosol from near-source sites

3.1 Data selection

Level 2 version 2 AERONET inversion data (Holben et al., 2006) from eight AERONET sites, shown in Fig. 1 (and with key information and references in Table 1), are used to investigate the microphysical properties of smoke aerosols over a range of different burning regimes. Some of these sites were previously used in a similar analysis by Dubovik et al. (2002); the analysis here benefits from a decade more observations, as well as improvements made to the version 2 AERONET database since that time (e.g. surface reflectance inputs; Eck et al., 2008). Giles et al. (2012) also examined a few of these sites, although that study was focussed on characterising global aerosol absorption properties from a variety of types, rather than creation and examination of microphysical models to represent these aerosols. State/country information for each site is given parenthetically the first time a given site is discussed in the text.

Some regions contain several sites in relatively close proximity; in this case, typically the site with the largest data record and smallest influence from other aerosol sources was chosen. Manual inspection reveals that data from these nearby sites are generally similar. For example, Mukdahan (Thailand) was chosen as a key site for south-eastern Asia, although quantitatively similar results are obtained if data from Pimai (also in Thailand) are used instead. Both sites primarily sample nearby agricultural burning, and forest burning from elsewhere in the region. In contrast, the site in the city of Chiang Mai (north-western Thailand) was not used as, while close to biomass burning source regions, it also has a significant urban contribution to the aerosol, coupled with the local topography leading to a "trapping" of pollutants (Gautam et al., 2012; Janjai et al., 2012). Another point to note is the omission of sites from the Sahel; although AERONET contains several long-term sites in this region, the dry season biomass burning peak here (November–February) due to burning of grassland, cropland, and shrubs coincides with strong dust activity, such that the aerosol is normally a mixture of biomass burning smoke and dust (Pandithurai et al., 2001; Roberts et al., 2009).

ACPD
13, 25013–25065, 2013

Johnson et al. (2008) and Eck et al. (2010) found cases where these smoke aerosols were highly absorbing, with midvisible SSA as low as 0.76, although the more common cases of mixed smoke and dust in this region are less absorbing. Limiting to smoke-dominant cases leaves a small data volume (and an unrepresentative sample of the true nature of the aerosol in that region). Additionally, the smoke and dust in this area often occur in distinct vertical layers and so a microphysical model based on column-average aerosol properties, when applied to real satellite data, could potentially be misleading or inaccurate (Kim et al., 2009). A similar rationale applies to sites in the Indo-Gangetic Plain and Himalayas (e.g. Pokhara, Nepal), as springtime biomass burning overlaps with transported dust, and some sites additionally have a significant urban component to the aerosol (Gautam et al., 2011).

At each site, in order to remove likely non-smoke cases from the data (as burning is seasonal and aerosol of other types may be transported periodically to sites), two sets of filters are applied. Firstly, it is required that $\tau_{440} \geq 0.4$ and $\alpha \geq 1$, to ensure reliability of retrieved refractive index/SSA and remove potential cases dominated by mineral dust aerosol (which has smaller α, e.g. Eck et al., 1999). Secondly, data are restricted to the main burning season for those sites where this is well-defined (see Table 1); some sites, such as Mongu (Zambia), exhibit fairly constant burning during throughout a period of several months, while others, such as Bonanza Creek (Alaska, USA), have a comparatively low baseline AOD punctuated by episodes of burning (which tend to occur in local summer months in dry years). As biomass burning is the dominant reason for high-AOD conditions at all these sites, the main effect of these filters is to remove some outlying results. Additionally, data from the year 2008 were excluded from CUIABA-MIRANDA (Mato Grosso, Brazil; hereafter Cuiaba), and from 2002 and 2004 from Jabiru (Australia), due to suspected instrumental issues which may affect retrieved SSA during these periods.

ACPD
13, 25013–25065, 2013

3.2 Overall and comparative microphysical/optical properties

3.2.1 Overview of summary Figures and Tables

The median retrieved volume size distributions corresponding to these biomass burning cases at each site are shown in Fig. 2. These reveal the presence of a strong fine mode with peak radius in the range 0.1–0.2 µm, and a secondary coarse mode with peak radius in the range 3–5 µm. Both modes appear approximately lognormal, although the coarse mode has a slight low-radius skew; the minimum in the overall aerosol volume size distribution is most commonly from 0.5–0.9 µm. On an individual-retrieval basis, and dependent upon the total AOD, the fine mode typically accounts for 40–90 % of the total aerosol volume (more at higher AOD) and 80–95 % of the AOD at 550 nm.

The AOD-dependence of aerosol size distribution parameters has previously been noted for a wide variety of aerosol types (e.g. Dubovik et al., 2002). Therefore, these data were also examined for these tendencies. An example of this process is shown in Fig. 3 for fine-mode radius and spread ($r_{v,f}$, σ_f) at Alta Floresta (Mato Grosso, Brazil). To mitigate the effect of outliers, size distribution parameters more than two standard deviations away from the median at a given site were discarded for this portion of the analysis, and then a linear least-squares fit of parameter against fine-mode AOD performed. The exclusion removed typically ~5 % of data, and did not lead to a significant difference in regression statistics, at most sites. Resulting linear regression relationships are shown in Table 2 for $\tau_{f,550}$ (and Table 3 for $\tau_{f,440}$, for reference), and illustrated later. The regression fits were performed against fine-mode AOD as this is likely a more reasonable metric of the contribution of biomass burning to the total aerosol burden. This is consistent with the primary emissions from biomass burning being small aerosol particles and aerosol precursor gases. For all sites the coarse-mode AOD was typically ~0.02-0.04 and roughly independent of the total AOD. Hence, similar results are obtained if total AOD is used instead. For a similar reason (low coarse-mode AOD and noisier size distribution parameters), no regression was performed for coarse-mode

ACPD
13, 25013–25065, 2013

size distribution parameters as a function of coarse AOD; instead, median values of $r_{v,c}$ and σ_c are given in Tables 2 and 3.

Aerosol refractive index was also found to be largely independent of AOD. The site-median refractive index, and SSA calculated using the relationships in Table 2 for the case of $\tau_{f,550} = 0.5$, $\tau_{c,550} = 0.03$ at each site, are given in Table 4. Although the AOD-dependence of model parameters means that SSA will itself be a factor of fine-mode AOD, the AOD-dependence of SSA is small according to these relationships (generally becoming less absorbing by ~0.01 as fine-mode AOD increases from 0.2–2).

The relationships between all these properties and total columnar water vapour were also explored, but in most cases omitted for brevity, due to a lack of observed covariability. This is consistent with the idea that biomass burning aerosols show weaker hygroscopicity than other fine-dominated aerosols (e.g. Reid et al., 2005a), and that ageing processes may have occurred rapidly and prior to the aerosols reaching the AERONET site. This could also be linked to the small gradient of the observed $\tau_{f,550}$-to-$r_{v,f}$ relationships at these sites, which are up to about an order of magnitude weaker than observed for more hygroscopic urban/industrial aerosol particles (e.g. Dubovik et al., 2002). Despite this, Reid et al. (2005a) did note that some measurements of biomass burning aerosols in scattered regions showed larger hygroscopic growth factors than expected, although the reasons for this were not understood. Additionally, as the AERONET aerosol and water vapour data represent column-averaged quantities they do not provide information about the extent of vertical overlap between aerosol and moisture. Changes due to moisture uptake may also be masked amongst variability of aerosol properties from other sources. One corollary of this is that, when using these parameters as a source of biomass burning aerosol microphysical properties for satellite AOD retrieval, it may not be necessary to account for hygroscopic growth of these particles for some burning types.

To facilitate a comparison between the different sites, Fig. 4 compares calculated size distributions and optical properties for the aforementioned case of $\tau_{f,550} = 0.5$, $\tau_{c,550} = 0.03$. Also shown are properties for the 'fine-dominated' aerosol model used

ACPD
13, 25013–25065, 2013

in the Sea-viewing Wide Field-of-view Sensor (SeaWiFS) Ocean Aerosol Retrieval (SOAR, Sayer et al., 2012a) algorithm, which is similar ($r_{\mathrm{eff,f}}$ within 0.03 µm, SSA lower by ~0.02–0.03) to models used in the operational over-ocean Moderate Resolution Imaging Spectroradiometer (MODIS; Remer et al., 2009) algorithm, and within the range of aerosol components included in the Multiangle Imaging Spectroradiometer (MISR; Kahn et al., 2010) algorithm.

3.2.2 Discussion of aerosol properties

Considering the above data, the eight sites span a range of size distributions and optical properties but there are some similarities between them. Bonanza Creek and Yakutsk (Siberia, Russia), both boreal forest/peat burning sites (likely mostly dominated by smouldering combustion), show the weakest and roughly spectrally-neutral absorption (ω_0 ~0.95), and are among the sites with a larger volume radius and broader distribution. Linear relationships between aerosol properties and AOD or water vapour at this site show strong scatter, but if plotted together as a function of day of year (Fig. 5), some seasonal tendencies become visible. Both $r_{\mathrm{v,f}}$ and σ_{f} tend to be larger for higher $\tau_{\mathrm{f,550}}$, which occurs most often in August at Bonanza Creek and more sporadically at Yakutsk. This is likely to soil drying through the season making peat soils more flammable through time (Eck et al., 2009, and references therein). There is a suggestion of a bowl-shaped profile of $r_{\mathrm{v,f}}$, with the lowest values from May–July and higher values earlier and later in the season. Columnar water vapour begins to increase around the start of June, and falls off during September. The SSA of the smoke is generally higher from mid-May onwards. It is possible that these seasonal changes reflect changes in moisture and/or vegetation phenology, resulting in a change of the nature of burning. Strong scatter is expected at these sites in particular as burning can occur across wide tracts of the land at these latitudes and be transported long distances, i.e. smoke sampled at these two sites may be of diverse origin and age.

In contrast, Cuiaba, Skukuza (South Africa), and Jabiru (grass, crop, and shrublands) are very similar to each other, with narrower lower-radius distributions, and are more

ACPD
13, 25013–25065, 2013

strongly absorbing (ω_0 ~0.88–0.9 in the visible, and ~0.85 in the near-infrared). Note that Cuiaba can also sample forest burning from the north, while Skukuza includes a sulphate contribution from industrial sources (Piketh et al., 1999). Mukdahan has a similar SSA to these sites, although size distribution shape and asymmetry parameter closer to Yakutsk. For this set of sites relationships between aerosol properties and water vapour were not evident, except at Mukdahan, where a weak increase (~0.03) in SSA from February to April was mirrored by an increase in water vapour during these inversions from ~2.5–4 cm. However this is likely linked to transport of air masses including pollutants from China/India, and an increase of forest burning relative to agricultural burning during this period, rather than hygroscopicity.

Intermediate between the properties of these two groups is Alta Floresta, which samples tropical woody burning from the nearby area. Relationships between aerosol fine-mode size/spread and water vapour (not shown) were found to be weak. The SSA at Cuiaba was found to be ~0.05 higher in October than August, while at the same time monthly median water vapour increased from ~2–4 cm; a similar change in water vapour at Alta Floresta through this period was not associated with any SSA change at this site. Together with the lack of change of size distribution parameters, this is consistent with the change in SSA at Cuiaba being driven with an increase in air masses containing transported smoke from forested regions through the season, rather than hygroscopicity. The overall lack of relationship with water vapour content is consistent with Schafer et al. (2008), who noted almost no dependence of AERONET aerosol properties on water vapour in Amazonia, except for the very highest AOD cases ($\tau_{550} > 1.5$). It is also worth noting that the area around the Alta Floresta site has become less forested due to agricultural conversion since the site was originally set up; analysis of the time series of retrieved aerosols properties at this site (not shown) reveals some interannual variability but no apparent trends or secular changes.

Aerosols at Mongu and Skukuza have similar size distribution properties, although the former is significantly more absorbing (SSA lower by about 0.05), likely due to the contribution from non-absorbing sulphates to the aerosol at Skukuza (Piketh et al.,

ACPD
13, 25013–25065, 2013

1999). Eck et al. (2013) found an increase in SSA of about 0.1 through the burning season at both of these sites (as well as inferred from AERONET at Etosha Pan, Namibia, and satellite observations), attributed to a likely decrease of black carbon content from May through to November due to sampling of fires from different fuel types. This temporal variability was also seen to manifest as temporal variability in bias of satellite-retrieved AOD. At both of these sites, water vapour was low (typically ~1–2 cm) and showed no links with aerosol properties.

The asymmetry parameter (g) is 0.68 ± 0.02 at 440 nm for all models (Fig. 4), but diverges to the range 0.43–0.57 at 1020 nm (due to the differences in fine/coarse AOD partition at longer wavelengths and fine mode aerosol size), again roughly along the lines of the groupings given previously. Similar values and spectral dependence for fine-dominated aerosols were found in previous analyses (e.g. Dubovik et al., 2002), while g for dust aerosols tends to show less spectral variability. In terms of spectral dependence of AOD, most models give about 140 % AOD at 440 nm relative to 550 nm, and 30 % at 1020 nm relative to 550 nm, yielding values of α across the midvisible in the range 1.8–2. The one outlier here is Bonanza Creek, for which this fine/coarse mode combination gives α=1.43, due to the larger and broader fine mode relative to the other sites. Note that although this linear α formulation is useful, it is only an approximation and caution should be taken when either using α to extrapolate AOD, or when comparing α determined across different wavelength ranges (e.g. Eck et al., 1999).

Examining the regression relationships in more detail, the fine-mode volume median radius for a moderate $\tau_{f,550}$ ~0.3 is typically ~0.14–0.15 µm for the aforementioned grass/shrubland sites and larger (0.15–0.2 µm) for the wood-burning sites. The gradient of the $\tau_{f,550}$-to-$r_{v,f}$ relationship is in the range 0.013–0.02 at most sites. Low to moderate correlations for these relationships (0.23 at Skukuza, up to 0.62 at Cuiaba) reflect both the low range of AOD spanned at some sites, possible contributions from other aerosol sources, and the fact that the scatter around these relationships (shown later) of order 0.01–0.02 is a similar size to the estimated uncertainty on AERONET retrievals of $r_{v,f}$

ACPD
13, 25013–25065, 2013

(mentioned previously). Similarly gradients and correlations with $\tau_{f,440}$ instead of $\tau_{f,550}$ are slightly lower as the same data and scatter are essentially being stretched across the AOD axis. Positive correlations between $\tau_{f,550}$ and σ_f are also observed, although are weak, likely for the same reasons of large scatter and limited dynamic range. All the above relationships are statistically significant at the 90 % level, except for τ_f vs. σ_f at Jabiru (although again, many relationships are numerically small). It is important to note that, although these relationships have been derived in a climatological sense, the scatter about them comprises a significant fraction of the observed variablility, due to both retrieval noise and sources of true natural variability.

Figure 6 shows that there is a fairly strong positive relationship between retrieved $r_{v,f}$ and σ_f ($r = 0.75$). This is true both across the ensemble of sites as a whole, as well as if sites are examined individually (not shown). As the uncertainty on each quantity can be significant compared to the data range, a bivariate linear fit (e.g. York, 1966) was used, with uncertainty on $r_{v,f}$ of 0.01 and on σ_f of 0.06. If the data are expressed in terms of number mean radius rather than volume (i.e. $r_{n,f}$ rather than $r_{v,f}$; Eq. 5), an opposing tendency is revealed: larger number mean radii are associated with narrower distributions, although the correlation is weaker (−0.46). A weaker correlation could in part be due to a larger uncertainty on the tails of the retrieved aerosol size distribution (Dubovik et al., 2000), to which $r_{n,f}$ is more sensitive than $r_{v,f}$. This anticorrelation was also observed across 36 observations of fresh and aged smoke collated by Janhäll et al. (2010). This could be caused by an initial broad distributions of emitted small particles coagulating into a narrower distribution of larger particles.

4 Smoke transport to coastal/island sites

Occasional cases of transported smoke have been observed at a wide range of coastal or island AERONET sites. Figure 7 shows smoke from several wildfires in California (USA), which are not uncommon in Northern Hemisphere summer and autumn, blown into the Pacific Ocean. Although not a rare occurrence, these sites are nonetheless

ACPD
13, 25013–25065, 2013

included in the "transported" rather than "near source" category in this analysis as there are insufficient cases passing over the AERONET sites to create a meaningful climatology of properties.

Figure 8 shows an example of more long-range transport, namely Amazonian smoke transported south through South America, eventually passing over the AERONET site in Buenos Aires (Argentina) and out into the southern Atlantic Ocean. This pathway is confirmed by the Hybrid Single Particle Lagrangian Integrated Trajectory (HYSPLIT; Draxler and Hess, 1998) model back-trajectory, for air arriving at Buenos Aires for ~2 km altitude (HYPSPLIT estimates of the altitude of this air mass near the source were 3–4.5 km). Aerosol properties at the sites in this figure are shown in more detail in Fig. 9: τ_{440} at Buenos Aires is low for most of the period, while at the other sites it is larger, approaching 4 at Alta Floresta, and more variable (Alta Floresta and Cuiaba lack observations prior to 18 August). High τ_{440} and α at these sites is consistent with biomass burning; the fine mode effective radius and SSA at Alta Floresta and Ji Paraná (Rondônia, Brazil) track each other reasonably closely, while the smoke at Cuiaba is slightly smaller and more absorbing. During 21–23 August, the plume is transported from the northern region to Buenos Aires (Fig. 8), and the SSA matches that at Alta Floresta/Ji Paraná (~0.9 at 440 nm), from where the plume is observed to travel. The absence of SSA retrievals outside this period at Buenos Aires is due to the low AOD (Dubovik et al., 2000). Note that the more-absorbing Cuiaba site lies outside of the main path of this plume. The fine mode effective radius at Buenos Aires is slightly larger during this period than before or after, and also larger than the near-source sites, which may be coincidental or may result from mixing with another air mass during transport. Following this event, AOD at Buenos Aires returns to typical low levels. Towards the end of the month satellite images (not shown) reveal that smoke from the forested region is blown over Cuiaba; the SSA and fine mode radius at Cuiaba increase to more closely match Alta Floresta/Ji Paraná.

Unfortunately, the number of cases where a smoke plume is observed at an AERONET site near-source and is conveniently transported past multiple other sites

ACPD
13, 25013–25065, 2013

over the course of days, thus providing the ability to track the evolution of the plume with AERONET, is very limited. Thus the comparison herein is more of a categorical nature: comparing how the body of case studies at island/coastal sites compares with the climatology and variability of land sites. Table 5 presents the list of AERONET inversions corresponding to such transported smoke identified at coastal/island sites (Fig. 1) used in this study. These data were individually identified as likely having a significant contribution from transported smoke by examination of satellite images, HYSPLIT back-trajectories, news/government agency reports, and guided by previous studies (Queface et al., 2003; O'Neill et al., 2005; Eck et al., 2009; Qin and Mitchell, 2009; Castro Videla et al., 2013).

Retrieved aerosol size distribution parameters and SSA for these cases are shown in Figs. 10, 11, 12, and 13, alongside those of the near-source AERONET sites which provide the closest match to these inversions. Properties for the "pure marine" aerosol model of Sayer et al. (2012b) are also shown for reference. This 'best match' was allocated subjectively, by identifying the source site for which the coastal/island site data in question lay most neatly within the cloud of points. For example, some cases at Buenos Aires are more similar to Alta Floresta, while others are more similar to Cuiaba, reflecting the different potential origins of the smoke. The main point is to illustrate that there is overlap between near-source and transported smoke aerosol properties, rather than to tie each individual case down to a specific burning type. Additionally, the fine mode radius/spread comparison is shown for the aggregate of these data points in Fig. 6. Similar relationships as for the near-source cases are observed, albeit with slightly different regression coefficients and weaker correlation, perhaps due to the more limited data range.

This comparison reveals that the fine-mode aerosol properties for these cases of smoke transported to ocean/coastal sites, in almost all cases, fall within the range of variability of smoke properties for the near-source sites. Some additional variability is observed, which could be attributed to additional ageing of the smoke aerosol particles and/or combination with aerosol particles from different air masses. In particular, most

ACPD
13, 25013–25065, 2013

of the coastal sites are in or near urban areas for which some additional urban/industrial aerosol contribution would be expected, as well as a potential marine aerosol contribution. Some of the matchups are not particularly surprising due to relative geographical proximity, e.g. Skukuza (South Africa) and Inhaca (Mozambique), or Jabiru and Darwin (Australia). Others, such as the similarity between properties at Cuiaba and the cases of Californian wildfires, are more noteworthy. The main conclusion from this is that microphysical models based on fine-mode smoke aerosol properties near source regions are also representative of smoke transported over the ocean, and so suitable for use in satellite AOD retrievals over ocean. Coarse-mode properties show more diversity between sites (and also often differ from pure marine aerosol properties), although as the coarse mode contribution to total AOD is minor this is not likely to be a significant source of error.

Despite the similarities identified between near-source and coastal/island transported smoke, there remain some notable differences. Inversions at the COVE site (off the coast of Virginia, USA) were for a case of smoke from Canadian boreal forest fires in July 2002 (O'Neill et al., 2005). In terms of fine mode radius and aerosol SSA, these show a similarity to the climatological properties of boreal forest burning at Bonanza Creek (and also Yakutsk; Figs. 10, 12). However, σ_f was smaller for these cases at COVE than commonly-observed at either of these sites. Additionally, there is comparatively large scatter in the observed fine-mode microphysical properties at these sites. This suggests that there may be significant variability in aerosol properties, perhaps influenced by variability in local conditions at the time of burning. A similarly large scatter is seen for Bach Long Vy (Fig. 12), in the Gulf of Tonkin (off the coast of Vietnam). Here it is likely that there is some urban/industrial component to the aerosol from nearby cities in Vietnam, flowing out of the Red River delta; this could explain the higher values of $r_{v,f}$ and σ_f at this site. Additionally, this site's location makes it more susceptible to instrumental degradation (e.g. moisture deposition and corrosion due to sea salt) than other sites, meaning retrievals may be less reliable here. A similar urban

ACPD
13, 25013–25065, 2013

contribution could explain the larger $r_{v,f}$ at Sevastopol (Ukraine) and Singapore than the comparison site of Yakutsk.

The largest outlier is Ascension Island, in the tropical Atlantic, which samples air masses including mixed Saharan/Sahelian dust and smoke aerosols from November–February, and central African smoke from June–October (only this second period contributed to the cases shown here). At this site, σ_f and aerosol SSA are a very close match to data from Mongu, while coarse-mode properties are similar to the pure maritime case (Fig. 11). However, $r_{v,f}$ is about 0.02 µm larger at Ascension Island than Mongu. This set of aerosol parameters is not a close match to any of the other near-source sites studied.

The Ascension Island site is fairly remote and in a harsh environment (exposed to salt from breaking waves, which may deposit on the instrument), which can lead to instrument problems more frequently than at some other AERONET sites. The most common symptom of these problems is an anomalously low SSA (typically up to 0.1 lower than expected). Errors in retrieved size distribution parameters (and direct-Sun spectral AOD) as a result of these problems are expected to be minor. For this reason, AERONET inversions from Ascension Island were subject to additional calibration/contamination checks beyond those applied for AERONET Level 2.0 processing as an extra precaution, and the data shown are for only those time periods where there was no indication of problems. Therefore it is likely that the higher $r_{v,f}$ at Ascension Island than Mongu is a real characteristic of the aerosol transported to this area, rather than an artefact. Potential reasons include, again, additional aerosol ageing in the time from emission to arrival at Ascension Island, as well as the possibility that properties of the freshly-emitted aerosol are different. Some air masses reaching Ascension Island pass over parts of Africa north of Mongu, which are more heavily forested (Roberts et al., 2009). Unfortunately, there are no AERONET sites in this region.

ACPD
13, 25013–25065, 2013

5 Implications for satellite AOD retrievals

Figure 4 revealed that the "fine-dominated" aerosol microphysical model used in over-ocean SeaWiFS processing (Sayer et al., 2012a) is intermediate in strength of absorption between the more weakly-absorbing boreal forest sites, and the more strongly-absorbing tropical forest and grass/shrubland sites. Therefore, use of this model to retrieve AOD from satellite measurements in these latter cases is likely to result in an underestimate of AOD (or conversely overestimate AOD for cases of weakly-absorbing smoke). The most absorbing fine-mode aerosol component in the widely-used MODIS operational processing over ocean is slightly less absorbing than this SeaWiFS model (Remer et al., 2009). This suggests that the over-ocean AOD from some regional smoke aerosols in these datasets, which are large and seasonally-repeating features in some parts of the world, but have been validated only sparsely due to a lack of ground truth data, may be understimated. In contrast the MISR aerosol mixtures include aerosols with a midvisible SSA down to about 0.8 (Kahn et al., 2010), which may be sufficient, if the retrieval algorithm is successful in choosing an appropriate mixture (although note again rare cases of even lower SSA; Johnson et al., 2008; Eck et al., 2010). All algorithms also include effectively nonabsorbing aerosol models. Although this discussion focusses on retrievals over ocean, it is worth mentioning for completeness that incorrect SSA also leads to biased AOD retrievals over land (e.g. Ichoku et al., 2003; Eck et al., 2013, for smoke examples).

Turning to observations, Fig. 14 compares midvisible AOD from these satellite products against AERONET data at Ascension Island. Data from November-February are excluded to minimise the contribution of transported dust, which happens in this season. The satellite:AERONET matchup protocol is as in Sayer et al. (2012a), namely AERONET data are spectrally interpolated to 550 nm and averaged within ±30 min of the satellite overpass, and satellite data are averaged within ±25 km of the AERONET site and restricted to only those retrievals meeting the dataset creators' recommended quality assurance flags. For $\tau_{550} > 0.3$ points, AERONET-derived α was most com-

ACPD
13, 25013–25065, 2013

monly ~1–1.6, consistent with mixed marine and smoke aerosols. The positive bias of MODIS and MISR data in low-AOD conditions (0–0.2) was noted in previous studies (Kahn et al., 2010, Sayer et al., 2012c). However, all datasets exhibit a low bias in AOD in conditions of elevated AOD, most notably SeaWiFS (although SeaWiFS has negligible bias in clean conditions while the others have a positive bias; the change in bias as AOD increases is more similar between all datasets).

To test the effect of aerosol absorption on satellite measurements, the 6S radiative transfer code (Vermote et al., 1997) was used to simulate TOA reflectance at wavelengths used for AOD retrieval by these sensors, for a variety of geometries, over an ocean surface with 6 ms^{-1} wind speed. Three aerosol types were considered: strongly-absorbing aerosol using the model for Mongu (Table 2, ω_0 ~0.85 at 440 nm); moderately-absorbing aerosol using the fine-dominated model of Sayer et al. (2012a) (ω_0 ~0.95 at 440 nm); and the pure marine model of Sayer et al. (2012b) (ω_0 ~0.99 at 440 nm). Then, for each wavelength simulated, these latter two models were used to retrieve AOD (reported relative to 550 nm) in each band, taking the Mongu case as 'truth', and so calculate the AOD retrieval error. Although this does not mirror how the individual satellite algorithms mentioned previously function, it does provide a direct comparative baseline of the sensitivity of each wavelength to the assumed strength of aerosol absorption.

Figure 15 illustrates the results of this test for a solar zenith angle of 45°, viewing zenith angle of 10°, and relative azimuth angle of 135°. Similar patterns are observed at other common Sun/sensor viewing geometries (not shown). This figure shows the increase of TOA reflectance with AOD, with the increase being less pronounced for more strongly-absorbing aerosols, leading to a low bias in retrieved AOD if the real aerosol is less absorbing than assumed. The difference is larger for shorter wavelengths, linked to the larger aerosol signal and increased Rayleigh-aerosol interactions. This lends support to the interpretation of Fig. 14, and suggests that future versions of satellite AOD retrieval algorithms should include an analogue for these strongly-absorbing aerosol particles.

ACPD
13, 25013–25065, 2013

Interestingly, although the current MISR algorithm includes strongly-absorbing aerosol mixtures, the change of bias from low-AOD to high-AOD conditions is similar to that in other sensors. This suggests that these mixtures may not always be chosen when needed (and the selection of an appropriate aerosol microphysical model to use in a system with a limited information content is a difficult problem in itself). The biases in high-AOD conditions in Fig. 14, typically from −0.1 to −0.3 for an AERONET AOD of 0.5, are similar in magnitude to those suggested in Fig. 15 as being due to insufficient absorption in the assumed aerosol properties. These results provide evidence that the assumed SSA may be to blame – although other aforementioned factors (e.g. surface reflectance, calibration, pixel selection) may also contribute.

6 Perspective

Biomass burning is one of the major contributors to the global aerosol burden, with both natural and anthropogenic sources. Analysis of AERONET retrievals of size distribution and refractive index revealed considerable variety between biomass burning aerosols in different global source regions, both in the size and strength of absorption of fine-mode particles. An advantage of AERONET is the long-term nature of observations at some sites, and consistency in observation, retrieval, and quality-assurance procedures between sites, making it a useful tool for comparisons of this type. Derived aerosol properties were found to be within a similar range to those observed in other studies by a variety of techniques. Additionally, case studies of transported smoke from a larger range of AERONET sites also frequently fell within the range of variability for these near-source sites.

Two broad "families" of aerosol properties were found, corresponding to boreal forests (comparatively larger, broader fine mode particles, with weaker and nearly spectrally-neutral absorption) and grass/shrub burning (smaller, narrower particles with stronger absorption, becoming more strongly-absorbing as wavelength increases from 440 nm to 1020 nm). Mongu in the southern African savannah exhibits even stronger

ACPD
13, 25013–25065, 2013

absorption, with average SSA around 0.85 in the midvisible. These families can serve as candidate sets of aerosol microphysical/optical properties for use in satellite AOD retrievals, which are reliant on assumptions about aerosol properties due to the limited information content available from existing passive spaceborne imaging radiometers. This does not, however, alleviate the difficulty of assuring that an appropriate microphysical model is used for any particular individual pixel-level satellite retrieval. The similarity between near-source and transported smoke properties implies that these models can be used for AOD retrieval over ocean, as well as land. These models represent the climatological properties of biomass burning at these sites, and cannot, however, capture the full range of variability at a given site.

An important outcome of this analysis is that the microphysical models adopted by commonly-used satellite AOD retrieval algorithms over ocean are insufficiently absorbing to represent aerosol optical properties well in many of these biomass-burning regimes. A consequence of this is that they are likely to underestimate the AOD in some smoke outflow regions. As these satellite datasets are increasingly used in climate applications, and as an evaluation tool for chemistry transport models, this is potentially a significant shortcoming. Rare cases of Sahelian smoke suggest that even stronger absorption may be seen (Johnson et al., 2008; Eck et al., 2010), which would further exacerbate these biases (although in this particular situation the smoke is almost always mixed with more weakly-absorbing dust). Until the launch of future satellite sensors with increased measurement capabilities, it is important that the continual evolution of algorithms using existing sensors includes the adoption of more realistic aerosol microphysical models as our knowledge of aerosol properties increases.

Acknowledgements. This work was supported by the NASA EOS program, managed by Hal Maring. The authors are grateful to the AERONET PIs and site managers (I. Abboud, R. Aguiar, P. Andryszczak, N. X. Anh, P. Arruda, P. Artaxo, E. Bernardino de Andrade, T. Bigala, J. de Brito Gomes, W. Brower, S. Campbell, P. Cesarano, G. Crooks, F. Denn, E. G. Dutton, R. D. Elia, B. Fabbri, R. Frouin, P. Glowacki, P. Greenwood, S. Halewood, N. M. Hoan, J. Hollingsworth, J. Ivanoff, M. Ives, D. Jatoba dos Santos, A. Jorge, D. M. Kabanov, G. Karasinski, K. L. Keong, M. E. Lee, S.-C. Liew, S. Meesiri, R. Mitchell, F. Morais, M. Mukulabai, N. Nelson, N. P. Ndhlovu,

ACPD
13, 25013–25065, 2013

S. Nikolashkin, C. B. Ning, A. Niyompam, E. Ojeda de Almeida Filho, N. O'Neill, L. Otero, M. Panchenko, S. Piketh, E. Quel, E. Reid, J. S. Reid, A. Royer, S. Sakerin, S. V. Salinas Cortijo, I. Sano, P. Sobolewski, J. de Souza Nogueira, G. A. Tolkachenko, G. Thomas, J. R. Vande Castle, R. Wagener, A. D. Webler, E. Wolfram, A. Yangthaisong, B. Zak) for the creation and stewardship of the ground-based data records used. MODIS data were obtained from the Level 1 and Atmosphere Archive and Distribution System (LAADS). F. Patadia, J. Limbacher, R. A. Kahn, and K. J. Mueller are thanked for assistance interpreting the MISR aerosol product file format. The authors gratefully acknowledge the NOAA Air Resources Laboratory (ARL) for the provision of the HYSPLIT transport and dispersion model and/or READY website (http://www.ready.noaa.gov) used in this publication. R. Gautam is acknowledged for useful discussions about Asian aerosols.

References

Aiken, A. C., Salcedo, D., Cubison, M. J., Huffman, J. A., DeCarlo, P. F., Ulbrich, I. M., Docherty, K. S., Sueper, D., Kimmel, J. R., Worsnop, D. R., Trimborn, A., Northway, M., Stone, E. A., Schauer, J. J., Volkamer, R. M., Fortner, E., de Foy, B., Wang, J., Laskin, A., Shutthanandan, V., Zheng, J., Zhang, R., Gaffney, J., Marley, N. A., Paredes-Miranda, G., Arnott, W. P., Molina, L. T., Sosa, G., and Jimenez, J. L.: Mexico City aerosol analysis during MILAGRO using high resolution aerosol mass spectrometry at the urban supersite (T0) – Part 1: Fine particle composition and organic source apportionment, Atmos. Chem. Phys., 9, 6633–6653, doi:10.5194/acp-9-6633-2009, 2009.

Ansmann, A., Petzold, A., Kandler, K., Tegen, I., Wendisch, M., Müller, D., Weinzierl, B., Müller, T., and Heintzenberg, J.: Saharan Mineral Dust Experiments SAMUM-1 and SAMUM-2: what have we learned?, Tellus B., 63, 403–429, doi:10.1111/j.1600-0889.2011.00555.x, 2011.

Artaxo, P., Martins, J. V., Yamasoe, M. A., Procópio, A. S., Pauliquevis, T. M., Andreae, M. O., Guyon, P., Gatti, L. V., and Leal, A. M. C.: Physical and chemical properties of aerosols in the wet and dry seasons in Rondônia, Amazonia, J. Geophys. Res., 107, 8081, doi:10.1029/2001JD000666, 2002.

Bridhikitti, A. and Overcamp, T. J.: Optical Characteristics of Southeast Asia's Regional Aerosols and Their Sources, J. Air Waste Management Assoc., 61, 747–754, doi:10.3155/1047-3289.61.7.747, 2011.

ACPD
13, 25013–25065, 2013

Bulgin, C. E., Palmer, P. I., Merchant, C. J., Siddans, R., Gonzi, S., Poulsen, C. A., Thomas, G. E., Sayer, A. M., Carboni, E., Grainger, R. G., Highwood, E. F., and Ryder, C. L.: Quantifying the response of the ORAC aerosol optical depth retrieval for MSG SEVIRI to aerosol model assumptions, J. Geophys. Res., 116, D05208, doi:10.1029/2010JD014483, 2011.

Castro Videla, F., Barnaba, F., Angelini, F., Cremades, P., and Gobbi, G. P.: The relative role of Amazonian and non-Amazonian fires in building up the aerosol optical depth in South America: A five year study (2005–2009), Atmos. Res., 122, 298–309, doi:10.1016/j.atmosres.2012.10.026, 2013.

Draxler, R. R. and Hess, G. D.: An overview of the HYSPLIT_4 modeling system of trajectories, dispersion, and deposition, Aust. Meteor. Mag., 47, 295–308, 1998.

Dubovik, O. and King, M. D.: A flexible inversion algorithm for retrieval of aerosol optical properties from Sun and sky radiance measurements, J. Geophys. Res., 105, doi:10.1029/2000JD900282, 20673–20696, 2000.

Dubovik, O., Smirnov, A., Holben, B. N., King, M. D., Kaufman, Y. J., Eck, T. F., and Slutsker, I.: Accuracy assessments of aerosol optical properties retrieved from Aerosol Robotic Network (AERONET) Sun and sky radiance measurements, J. Geophys. Res., 105, 9791–9806, 2000.

Dubovik, O., Holben, B., Eck, T. F., Smirnov, A., Kaufman, Y., King, M., Tanré, D., and Slutsker, I.: Variability and optical properties of key aerosol types observed in worldwide locations, J. Atm. Sci., 59, 590–608, doi:10.1175/1520-0469(2002)059<0590:VOAAOP>2.0.CO;2, 2002.

Dubovik, O., Sinyuk, A., Lapyonok, T., Holben, B., Mischenko, M., Yang, P., Eck, T., Volten, H., Muñoz, O., Veihelmann, B., van der Zande, W. J., Leon, J.-F., Sorokin, M., and Slutsker, I.: The application of spheroid models to account for aerosol particle non-sphericity in remote sensing of desert dust, J. Geophys. Res., 111, doi:10.1029/2005JD006619, 2006.

Dubovik, O., Herman, M., Holdak, A., Lapyonok, T., Tanré, D., Deuzé, J. L., Ducos, F., Sinyuk, A., and Lopatin, A.: Stastically optimized inversion algorithm for enhanced retrieval of aerosol properties from spectral multi-angle polarimetric satellite observations, Atmos. Meas. Tech., 4, 975–1018, doi:10.5194/amt-4-975-2011, 2011.

Eck, T. F., Holben, B. N., Reid, J. S., Dubovik, O., Smirnov, A., O'Neill, N. T., Slutsker, I., and Kinne, S.: Wavelength dependence of the optical depth of biomass burning, urban, and desert dust aerosols, J. Geophys. Res., 104, 31333–31349, 1999.

Eck, T. F., Holben, B. N., Ward, D. E., Dubovik, O., Reid, J. S., Smirnov, A., Mukelabai, M. M., Hsu, N. C., O'Neill, N. T., and Slutsker, I.: Characterization of the optical properties of

ACPD
13, 25013–25065, 2013

biomass burning aerosols in Zambia during the 1997 ZIBBEE field campaign, J. Geophys. Res., 106, 3425–3448, doi:10.1029/2000JD900555, 2001.

Eck, T. F., Holben, B. N., Ward, D. E., Mukelabai, M. M., Dubovik, O., Smirnov, A., Schafer, J. S., Hsu, N. C., Piketh, S. J., Quedace, A., Le Roux, J., Swap, R. J., and Slutsker, I.: Variability of biomass burning aerosol optical characteristics in southern Africa during the SAFARI 2000 dry season campaign and a comparison of single scattering albedo estimates from radiometric measurements, J. Geophys. Res., 108, 8477, doi:10.1029/2002JD002321, 2003.

Eck, T. F., Holben, B. N., Reid, J. S., Sinyuk, A. Dubovik, O., Smirnov, A., Giles, D. M., O'Neill, N. T., Tsay, S.-C., Ji, Q., Al Mandoos, A., Ramzan Khan, M., Reid, E. A., Schader, J. S., Sorokin, M., Newcomb, W., and Slusker, I.: Spatial and temporal variability of column-integrated aerosol optical properties in the southern Arabian Gulf and United Arab Emirates in summer, J. Geophys. Res., 113, D01204, doi:10.1029/2007JD008944, 2008.

Eck, T. F., Holben, B. N., Reid, J. S., Sinyuk, A., Hyer, E. J., O'Neill, N. T., Shaw, G. E., Vande Castle, J. R., Chapin, F. S., Dubovik, O., Smirnov, A., Vermote, E., Schafer, J. S., Giles, D., Slutsker, I., Sorokine, M., and Newcomb, W. W.: Optical properties of boreal region biomass burning aerosols in central Alaska and seasonal variation of aerosol optical depth at an Arctic coastal site, J. Geophys. Res., 114, D11201, doi:10.1029/2008JD010870, 2009.

Eck, T. F., Holben, B. N., Sinyuk, A., Pinker, R. T., Goloub, P., Chen, H., Chatenet, B., Li, Z., Singh, R. P., Tripathi, S. N., Reid, J. S., Giles, D. M., Dubovik, O., O'Neill, N. T., Smirnov, A., Wang, P., and Xia, X.: Climatological aspects of the optical properties of fine/coarse mode aerosol mixtures, J. Geophys. Res., 115, D19205, doi:10.1029/2010JD014002, 2010.

Eck, T. F., Holben, B. N., Reid, J. S., Mukelabai, M. M., Piketh, S. J., Torres, O., Jethva, H. T., Hyer, E. J., Ward, D. E., Dubovik, O., Sinyuk, A., Schafer, J. S., Giles, D. M., Sorokin, M., Smirnov, A., and Slutsker, I.: A seasonal trend of single scattering albedo in southern African biomass-burning particles: Implications for satellite products and estimates of emissions for the world's largest biomass-burning source, J. Geophys. Res., 118, 5380–5552, doi:10.1002/jgrd.50500, 2013.

Gautam, R., Hsu, N. C., Tsay, S.-C., Lau, W. K., Holben, B., Bell, S., Smirnov, A., Li, C., Hansell, R., Ji, Q., Payra, S., Aryal, D., Kayastha, R., and Kim, K. M.: Accumulation of aerosols over the Indo-Gangetic plains and southern slopes of the Himalayas: distribution, properties and radiative effects during the 2009 pre-monsoon season, Atmos. Chem. Phys., 11, 12841–12863, doi:10.5194/acp-11-12841-2011, 2011.

ACPD
13, 25013–25065, 2013

Gautam, R., Hsu, N. C., Eck, T. F., Holben, B. N., Janjai, S., Jantarach, T., Tsay, S.-C., and Lau, W. K.: Characterization of aerosols over the Indochina peninsula from satellite-surface observations during biomass burning pre-monsoon season, Atmos. Environ., 78, 51–59, doi:10.1016/j.atmosenv.2012.05.038, 2013.

Giles, D. M., Holben, B. N., Tripathi, S. N., Eck, T. F., Newcomb, W. W., Slutsker, I., Dickerson, R. R., Thompson, A. M., Mattoo, S., Wang, S.-H., Singa, R. P., Sinyuk, A., and Schafer, J. S.: Aerosol properties over the Indo-Gangetic Plain: A mesoscale perspective from the TIGERZ experiment, J. Geophys. Res., 116, D18203, doi:10.1029/2011JD015809, 2011.

Giles, D. M., Holben, B. N., Eck, T. F., Sinyuk, A., Smirnov, A., Slutsker, I., Dickerson, R. R., Thompson, A. M., and Schafer, J. S.: An analysis of AERONET aerosol absorption properties and classifications representative of aerosol source regions, J. Geophys. Res., 117, D17203, doi:10.1029/2012JD018127, 2012.

Hasekamp, O., Litvinov, P., and Butz, A.: Aerosol properties over the ocean from PARASOL multi-angle photopolarimetric measurements, J. Geophys. Res., 116, D14204, doi:10.1029/2010JD015469, 2011.

Hasekamp, O. P. and Landgraf, J.: Retrieval of aerosol properties over the ocean from multispectral single-viewing-angle measurements of intensity and polarization: Retrieval approach, information content, and sensitivity study, J. Geophys. Res., 110, D20207, doi:10.1029/2005JD006212, 2005.

Hobbs, P. V., Reid, J. S., Herring, J. A., Nance, J. D., Weiss, R. E., Ross, J. L., Hegg, D. A., Ottmar, R. D., and Liousse, C. A.: Particle and trace-gas measurements in the smoke from prescribed bums of forest products in the Pacific Northwest, MIT Press, in: Global Biomass Burning and Global Change, edited by: Levine, J. S., 1997.

Holben, B. N., Eck, T. F., Slutsker, I., Tanré, D., Buis, J. P., Setzer, A., Vermote, E., Reagan, J. A., Kaufman, Y. J., Nakajima, T., Lavenu, F., Jankowiak, I., and Smirnov, A.: AERONET: A federated instrument network and data archive for aerosol characterization, Remote Sens. Environ., 66, 1–16, doi:10.1016/S0034-4257(98)00031-5, 1998.

Holben, B. N., F., E. T., Slustker, I., Smirnov, A., Sinyuk, A., Shafer, J., Giles, D., and Dubocik, O.: AERONET's version 2.0 quality assurance criteria, in: Proceedings of SPIE, 6408, paper no. 6408-27, 2006.

Ichoku, C., Remer, L. A., Kaufman, Y. J., Levy, R., Chu, D. A., Tanré, D., and Holben, B. N.: MODIS observation of aerosols and estimation of aerosol radiative forcing over south-

ACPD
13, 25013–25065, 2013

ern Africa during SAFARI 2000, J. Geophys. Res., 108, 8499, doi:10.1029/2002JD002366, 2003.
Janhäll, S., Andreae, M. O., and Pöschl, U.: Biomass burning aerosol emissions from vegetation fires: particle number and mass emission factors and size distributions, Atmos. Chem. Phys., 10, 1427–1439, doi:10.5194/acp-10-1427-2010, 2010.
Janjai, S., Nunuez, M., Masiri, I., Wattan, R., Buntoung, S., Jantarach, T., and Promsen, W.: Aerosol optical properties at Four Sites in Thailand, Atmos. Clim. Sci, 2, 441–453, doi:10.4236/acs.2012.24038, 2012.
Johnson, B. T., Osborne, S. R., Haywood, J. M., and Harrison, M. A. J.: Aircraft measurements of biomass burning aerosol over West Africa during DABEX, J. Geophys. Res., 113, D00C06, doi:10.1029/2007JD009451, 2008.
Kahn, R., West, R., McDonald, D., Rheingans, B., and Mischenko, M. I.: Sensitivity of multiangle remote sensing observations to aerosol sphericity, J. Geophys. Res., 102, 16861–16870, doi:10.1029/96JD01934, 1997.
Kahn, R., Garay, M. J., Nelson, D. L., Yau, K. K., Bull, M. A., Gaitley, B. J., Martonchik, J. V., and Levy, R.: Satellite-derived aerosol optical depth over dark water from MISR and MODIS: Comparisons with AERONET and implications for climatological studies, J. Geophys. Res., 112, D18205, doi:10.1029/2006JD008175, 2007.
Kahn, R. A., Gaitley, B. J., Garay, M. J., Diner, D. J., Eck, T. F., Smirnov, A., and Holben, B. N.: Multiangle Imaging SpectroRadiometer global aerosol product assessment by comparison with the Aerosol Robotic Network, J. Geophys. Res., 115, D23209, doi:10.1029/2010JD014601, 2010.
Kaufman, Y. J., Hobbs, P. V., Kirchoff, V. W. J. H., Artaxo, P., Remer, L. A., Holben, B. N., King, M. D., Ward, D. E., Prins, E. M., Longo, K. M., Mattos, L. F., Nobre, C. A., Spinhirne, J. D., Hl, Q., Thompson, A. M., Gleason, J. F., Christopher, S. A., and Tsay, S.-C.: Smoke, Clouds, and Radiation-Brazil (SCAR-B) experiment, J. Geophys. Res., 103, 31783–31808, doi:10.1029/98JD02281, 1998.
Kaufman, Y. J., Remer, L. A., Tanré, D., Li, R.-R., Kleidman, R., Mattoo, S., Levy, R. C., Eck, T. F., Holben, B. N., Ichoku, C., Martins, J. V., and Koren, I.: A Critical Examination of the Residual Cloud Contamination and Diurnal Sampling Effects on MODIS Estimates of Aerosol Over Ocean, IEEE Trans. Geosci. Remote Sens., 43, 2886–2897, doi:10.1109/TGRS.2005.858430, 2005.

ACPD
13, 25013–25065, 2013

Kim, S.-W., Chazette, P., Dulac, F., Sanak, J., Johnson, B., and Yoon, S.-C.: Vertical structure of aerosols and water vapor over West Africa during the African monsoon dry season, Atmos. Chem. Phys., 9, 8017–8038, doi:10.5194/acp-9-8017-2009, 2009.
Kokhanovsky, A. A., Deuzé, J. L., Diner, D. J., Dubovik, O., Ducos, F., Emde, C., Garay, M. J., Grainger, R. G., Heckel, A., Herman, M., Katsev, I. L., Keller, J., Levy, R., North, P. R. J., Prikhach, A. S., Rozanov, V. V., Sayer, A. M., Ota, Y., Tanré, D., Thomas, G. E., and Zege, E. P.: The determination of spectral aerosol optical thickness from satellites: an inter-comparison of algorithms using synthetic backscattered solar light characteristics, Atmos. Meas. Tech., 3, 909–932, doi:10.5194/amt-3-909-2010, 2010.
Lee, J., Kim, J., Yang, P., and Hsu, N. C.: Improvement of aerosol optical depth retrieval from MODIS spectral reflectance over the global ocean using new aerosol models archived from AERONET inversion data and tri-axial ellipsoidal dust database, Atmos. Chem. Phys., 12, 7087–7102, doi:10.5194/acp-12-7087-2012, 2012.
Levy, R. C., Leptoukh, G. G., Kahn, R., Zubko, V., Gopalan, A., and Remer, L. A.: A Critical Look at Deriving Monthly Aerosol Optical Depth From Satellite Data, IEEE Trans. Geosci. Remote Sens., 47, 2942–2956, doi:10.1109/TGRS.2009.2013842, 2009.
Magi, B. I. and Hobbs, P. V.: Effects of humidity on aerosols in southern Africa during the biomass burning season, J. Geophys. Res., 108, 8495, doi:10.1029/2002JD002144, 2003.
Martins, J. V., Artaxo, P., Hobbs, P. V., Liousse, C., Cachier, H., Kaufman, Y., and Plana-Fattoria, A.: Particle size distributions, elemental compositions, carbon measurements, and optical properties of smoke from biomass burning in the Pacific Northwest of the United States, MIT Press, in: Global Biomass Burning and Global Change, edited by: Levine, J. S., 1997.
Martonchik, J. V., Diner, D. J., Kahn, R. A., Ackerman, T. P., Verstraete, M. M., Pinty, B., and Gordon, H. R.: Techniques for the retrieval of aerosol properties over land and ocean using multi-angle imaging, IEEE Trans. Geosci. Remote Sens., 36, 1212–1227, doi:10.1109/36.701027, 1998.
McConnell, C. L., Highwood, E. J., Coe, H., Formenti, P., Anderson, B., Osborne, S., Nava, S., Desbouefs, K., Chen, G., and Harrison, M. A. J.: Seasonal variations of the physical and optical characteristics of Saharan dust: Results from the Dust Outflow and Deposition to the Ocean (DODO), J. Geophys. Res., 113, D14S05, doi:10.1029/2007JD009606, 2008.
McMeeking, G. R., Morgan, W. T., Flynn, M., Highwood, E. J., Turnbull, K., Haywood, J., and Coe, H.: Black carbon aerosol mixing state, organic aerosols and aerosol optical properties

ACPD
13, 25013–25065, 2013

over the United Kingdom, Atmos. Chem. Phys., 11, 9037–9052, doi:10.5194/acp-11-9037-2011, 2011.
Mishchenko, M. I., Travis, L. D., Kahn, R. A., and West, R. A.: Modeling phase functions for dustlike tropospheric aerosols using a shape mixture of randomly oriented polydisperse spheroids, J. Geophys. Res., 102, 16831–16847, doi:10.1029/96JD02110, 1997.
Mishchenko, M. I., Geogdzhayev, I. V., Cairns, B., Rossow, W. B., and Lacis, A. A.: Aerosol retrievals over the ocean by use of channels 1 and 2 AVHRR data: sensitivity analysis and preliminary results, Appl. Opt., 38, 7325–7341, doi:10.1364/AO.38.007325, 1999.
O'Dowd, C. D. and de Leeuw, G.: Marine aerosol production: a review of the current knowledge, Phil. Trans. R. Soc. A, 365, doi:10.1098/rsta.2007.2043, 2007.
O'Neill, N. T., Thulasiraman, S., Eck, T. F., and Reid, J. S.: Robust optical features of fine mode size distributions: Application to the Québec smoke event of 2002, J. Geophys. Res., 110, D11207, doi:10.1029/2004JD005157, 2005.
Pandithurai, G., Pinker, R. T., Dubovik, O., Holben, B. N., and Aro, T.: Remote sensing of aerosol optical characteristics in sub-Sahel, West Africa, J. Geophys. Res., 106, 28347–28356, doi:10.1029/2001JD900234, 2001.
Paris, J.-D., Stohl, A., Nédélec, P., Arshinov, M. Y., Panchenko, M. V., Shmargunov, V. P., Law, K. S., Belan, B. D., and Ciais, P.: Wildfire smoke in the Siberian Arctic in summer: source characterization and plume evolution from airborne measurements, Atmos. Chem. Phys., 9, 9315–9327, doi:10.5194/acp-9-9315-2009, 2009.
Piketh, S. J., Annegarn, H. J., and Tyson, P. D.: Lower tropospheric aerosol loadings over South Africa: The relative contribution of aeolian dust, industrial emissions, and biomass burning, J. Geophys. Res., 104, 1597–1607, doi:10.1029/1998JD100014, 1999.
Qin, Y. and Mitchell, R. M.: Characterisation of episodic aerosol types over the Australian continent, Atmos. Chem. Phys., 9, 1943–1956, doi:10.5194/acp-9-1943-2009, 2009.
Queface, A. J., Piketh, S. J., Annegarn, H. J., Holben, B. N., and Uthui, R. J.: Retrieval of aerosol optical thickness and size distribution from the CIMEL Sun photometer over Inhaca Island, Mozambique, J. Geophys. Res., 108, 8509, doi:10.1029/2002JD002374, 2003.
Queface, A. J., Piketh, S. J., Eck, T. F., Tsay, S.-C., and Mavume, A. F.: Climatology of aerosol optical properties in Southern Africa, Atmos. Env., 45, 2910–2921, doi:10.1016/j.atmosenv.2011.01.056, 2011.
Radke, L. F., Hegg, D. A., Hobbs, P. V., Nance, J. D., Lyons, J. H., Laursen, K. K., Weiss, R. E., Riggan, P. J., and Ward, D. E.: Particulate and Trace Gas Emissions from Large Biomass

ACPD
13, 25013–25065, 2013

Fires in North America, MIT Press, in: Global Biomass Burning: Atmospheric, Climatic, and Biopheric Implications, edited by: Levine, J. S., 1991.
Reid, J. S. and Hobbs, P. V.: Physical and optical properties of young smoke from individual biomass fires in Brazil, J. Geophys. Res., 103, 32013–32030, doi:10.1029/98JD00159, 1998.
Reid, J. S., Eck, T. F., Christopher, S. A., Koppmann, R., Dubovik, O., Eleuterio, D. P., Holben, B. N., Reid, E. A., and Zhang, J.: A review of biomass burning emissions part III: intensive optical properties of biomass burning particles, Atmos. Chem. Phys., 5, 827–849, doi:10.5194/acp-5-827-2005, 2005a.
Reid, J. S., Koppmann, R., Eck, T. F., and Eleuterio, D. P.: A review of biomass burning emissions part II: intensive physical properties of biomass burning particles, Atmos. Chem. Phys., 5, 799–825, doi:10.5194/acp-5-799-2005, 2005b.
Remer, L. A., Kleidman, R. G., Levy, R. C., Kaufman, Y. J., Tanré, D., Mattoo, S., Martins, J. V., Ichoku, C., Koren, I., Yu, H., and Holben, B. N.: Global aerosol climatology from the MODIS satellite sensors, J. Geophys. Res., 113, D14S07, doi:10.1029/2007JD009661, 2008.
Remer, L. A., Tanré, D., and Kaufman, Y. J.: Algorithm for remote sensing of tropospheric aerosol from MODIS: Collection 5, Tech. rep., NASA Goddard Space Flight Center, ATBD-MOD-02, product ID MOD04/MYD04, available online from http://modis.gsfc.nasa.gov/data/atbd/ (last access: July 2013), 2009.
Roberts, G., Wooster, M. J., and Lagoudakis, E.: Annual and diurnal African biomass burning temporal dynamics, Biogeosciences, 6, 849–866, doi:10.5194/bg-6-849-2009, 2009.
Ryder, C. L., Highwood, E. J., Rosenberg, P. D., Trembath, J., Booke, J. K., Bart, M., Dean, A., Crosier, J., Dorsey, J., Brindley, H., Banks, J., Masrham, J. H., McQuiad, J. B., Sodemann, H., and Washington, R.: Optical properties of Saharan dust aerosol and contribution from the coarse mode as measured during the Fennec 2011 aircraft campaign, Atmos. Chem. Phys., 13, 303–325, doi:10.5194/acp-13-303-2013, 2013.
Sayer, A. M., Thomas, G. E., and Grainger, R. G.: A sea surface reflectance model for (A)ATSR, and application to aerosol retrievals, Atmos. Meas. Tech., 3, 813–838, doi:10.5194/amt-3-813-2010, 2010a.
Sayer, A. M., Thomas, G. E., Palmer, P. I., and Grainger, R. G.: Some implications of sampling choices on comparisons between satellite and model aerosol optical depth fields, Atmos. Chem. Phys., 10, 10705–10716, doi:10.5194/acp-10-10705-2010, 2010b.

ACPD
13, 25013–25065, 2013

Sayer, A. M., Hsu, N. C., Bettenhausen, C., Ahmad, Z., Holben, B. N., Smirnov, A., Thomas, G. E., and Zhang, J.: SeaWiFS Ocean Aerosol Retrieval (SOAR): Algorithm, validation, and comparison with other datasets, J. Geophys. Res, 117, D03206, doi:10.1029/2011JD016599, 2012a.

Sayer, A. M., Smirnov, A., Hsu, N. C., and Holben, B. N.: A pure marine aerosol model, for use in remote sensing applications, J. Geophys. Res., 117, D05213, doi:10.1029/2011JD016689, 2012b.

Sayer, A. M., Smirnov, A., Hsu, N. C., Munchak, L. A., and Holben, B. N.: Estimating marine aerosol particle volume and number from Maritime Aerosol Network data, Atmos. Chem. Phys., 12, 8889–8909, doi:10.5194/acp-12-8889-2012, 2012c.

Schafer, J. S., Eck, T. F., Holben, B. N., Artaxo, P., and Duarte, A. F.: Characterization of the optical properties of atmospheric aerosols in Amazônia from long-term AERONET monitoring (1993–1995 and 1999–2006), J. Geophys. Res., 113, D04204, doi:10.1029/2007JD009319, 2008.

Smirnov, A., Holben, B. N., Eck, T. F., Dubovik, O., and Slutsker, I.: Cloud-screening and quality control algorithms for the AERONET database, Remote Sens. Environ., 73, 337–349, 2000.

Streets, D. G., Yarber, K. F., Woo, J.-H., and Carmichael, G. R.: Biomass burning in Asia: Annual and seasonal estimates and atmospheric emissions, Global Biogeochem. Cy., 17, 1099, doi:10.1029/2003GB002040, 2003.

Su, L. and Toon, O. B.: Saharan and Asian dust: similarities and differences determined by CALIPSO, AERONET, and a coupled climate-aerosol microphysical model, Atmos. Chem. Phys., 11, 3263–3280, doi:10.5194/acp-11-3263-2011, 2011.

Swap, R. J., Annegarn, H. J., Suttles, J. T., King, M. D., Platnick, S., Privette, J. L., and Scholes, R. J.: Africa burning: A thematic analysis of the Southern African Regional Science Initiative (SAFARI 2000), J. Geophys. Res., 108, 8465, doi:10.1029/2003JD003747, 2003.

Thomas, G. E., Poulsen, C. A., Sayer, A. M., Marsh, S. H., Dean, S. M., Carboni, E., Siddans, R., Grainger, R. G., and Lawrence, B. N.: The GRAPE aerosol retrieval algorithm, Atmos. Meas. Tech., 2, 679–701, doi:10.5194/amt-2-679-2009, 2009.

Vermote, E. F., Tanré, D., Deuzé, J. L., Herman, M., and Morcrette, J.-J.: Second Simulation of the Satellite Signal in the Solar Spectrum, 6S: An Overview, IEEE Trans. Geosci. Remote Sens., 35, 675–686, doi:10.1109/36.581987, 1997.

York, D.: Least-squares fitting of a straight line, Can. J. Phys., 44, 1079–1086, doi:10.1139/p66-090, 1966.

ACPD
13, 25013–25065, 2013

Table 1. Geographical/sampling information for biomass-burning AERONET land sites, along with key references for burning in these regions.

Site	Latitude, degrees	Longitude, degrees	Elevation m.a.s.l.	Burning season	Range of years	Number of retrievals	Key references
Alta Floresta	−9.87100	−56.1040	277	August–October	1999–2011	621	Kaufman et al. (1998), Artaxo et al. (2002), Dubovik et al. (2002), Schafer et al. (2008)
Bonanza Creek	64.7430	−148.316	150	–	1999–2010	156	Eck et al. (2009)
Cuiaba	−15.7290	−56.0210	210	September–October	2001–2011	436	Kaufman et al. (1998), Dubovik et al. (2002),Schafer et al. (2008)
Jabiru	−12.6610	132.893	30	–	2003–2011	117	Qin and Mitchell (2009)
Mongu	−15.2540	23.1510	1107	July–October	1999–2009	1435	Eck et al. (2001), 2003, 2013, Magi and Hobbs (2003), Swap et al. (2003), Queface et al. (2011)
Mukdahan	16.6070	104.676	166	February–April	2004–2009	723	Bridhikitti and Overcamp (2011), Gautam et al. (2012), Janjai et al. (2012)
Skukuza	−24.9920	31.5870	150	July–October	1999–2010	422	Eck et al. (2003), Magi and Hobbs (2003), Swap et al. (2003), Queface et al. (2011)
Yakutsk	61.6620	129.367	118	–	2004–2012	103	Paris et al. (2009)

ACPD
13, 25013–25065, 2013

Table 2. Size distribution parameters for biomass burning aerosols from the climatological AERONET smoke sites (relative to fine/coarse AOD at 550 nm). Note that the fine-mode volume relationship is calculated for $\tau_{f,550} = 0.5$ as in Fig. 4 and so will vary for different AOD. r indicates Pearson's linear correlation coefficient.

Site	Maximum $\tau_{f,550}$	$C_{v,f}$, $\mu m^3\,\mu m^{-2}$	$r_{v,f}$ μm	σ_f	$C_{v,c}$ $\mu m^3\,\mu m^{-2}$	$r_{v,c}$ μm	σ_c
Alta Floresta	2.43	$0.188\tau_{f,550}$	$0.148+0.013\tau_{f,550}$, $r = 0.44$	$0.383 +0.035\tau_{f,550}$, $r = 0.41$	$1.52\tau_{c,550}$	3.20	0.65
Bonanza Creek	2.58	$0.140\tau_{f,550}$	$0.191+0.020\tau_{f,550}$, $r = 0.44$	$0.519 +0.016\tau_{f,550}$, $r = 0.19$	$1.47\tau_{c,550}$	3.20	0.69
Cuiaba	2.23	$0.190\tau_{f,550}$	$0.136+0.025\tau_{f,550}$, r=0.62	$0.368 +0.048\tau_{f,550}$, $r = 0.50$	$1.60\tau_{c,550}$	3.28	0.62
Jabiru	0.586	$0.220\tau_{f,550}$	$0.133+0.044\tau_{f,550}$, $r = 0.32$	$0.372 +0.017\tau_{f,550}$, $r = 0.05$	$1.06\tau_{c,550}$	2.38	0.73
Mongu	1.48	$0.170\tau_{f,550}$	$0.133+0.026\tau_{f,550}$, $r = 0.46$	$0.369 +0.049\tau_{f,550}$, $r = 0.29$	$1.57\tau_{c,550}$	3.34	0.67
Mukdahan	1.51	$0.182\tau_{f,550}$	$0.157+0.039\tau_{f,550}$, $r = 0.44$	$0.426 +0.066\tau_{f,550}$ $r = 0.33$	$1.41\tau_{c,550}$	2.96	0.63
Skukuza	1.00	$0.204\tau_{f,550}$	$0.138+0.018\tau_{f,550}$, $r = 0.23$	$0.361 +0.031\tau_{f,550}$ $r = 0.16$	$1.26\tau_{c,550}$	2.80	0.69
Yakutsk	2.74	$0.173\tau_{f,550}$	$0.164+0.017\tau_{f,550}$, $r = 0.35$	$0.464 +0.040\tau_{f,550}$, $r = 0.30$	$1.49\tau_{c,550}$	3.34	0.72

ACPD
13, 25013–25065, 2013

Table 3. As Table 2, except expressed in terms of AOD at 440 nm.

Site	Maximum $\tau_{f,440}$	$C_{v,f}$, $\mu m^3\ \mu m^{-2}$	$r_{v,f}$ μm	σ_f	$C_{v,c}$ $\mu m^3\ \mu m^{-2}$	$r_{v,c}$ μm	σ_c
Alta Floresta	3.78	$0.126\tau_{f,440}$	$0.148 + 0.0083\tau_{f,440}$, $r = 0.41$	$0.383 + 0.022\tau_{f,440}$, $r = 0.40$	$1.55\tau_{c,440}$	3.20	0.65
Bonanza Creek	3.69	$0.108\tau_{f,440}$	$0.193 + 0.013\tau_{f,440}$, $r = 0.39$	$0.520 + 0.011\tau_{f,440}$, $r = 0.18$	$1.50\tau_{c,440}$	3.20	0.69
Cuiaba	3.28	$0.128\tau_{f,440}$	$0.136 + 0.016\tau_{f,440}$, $r = 0.61$	$0.367 + 0.031\tau_{f,440}$, $r = 0.49$	$1.62\tau_{c,440}$	3.28	0.62
Jabiru	0.877	$0.147\tau_{f,440}$	$0.134 + 0.027\tau_{f,440}$, $r = 0.30$	$0.372 + 0.0096\tau_{f,440}$, $r = 0.05$	$1.09\tau_{c,440}$	2.48	0.73
Mongu	2.29	$0.115\tau_{f,440}$	$0.133 + 0.016\tau_{f,440}$, $r = 0.43$	$0.369 + 0.031\tau_{f,440}$, $r = 0.28$	$1.60\tau_{c,440}$	3.34	0.67
Mukdahan	2.11	$0.129\tau_{f,440}$	$0.159 + 0.024\tau_{f,440}$, $r = 0.39$	$0.429 + 0.041\tau_{f,440}$, $r = 0.30$	$1.44\tau_{c,440}$	2.96	0.63
Skukuza	1.57	$0.137\tau_{f,440}$	$0.138 + 0.010\tau_{f,440}$, $r = 0.20$	$0.362 + 0.017\tau_{f,440}$, $r = 0.14$	$1.29\tau_{c,440}$	2.80	0.69
Yakutsk	3.89	$0.120\tau_{f,440}$	$0.164 + 0.011\tau_{f,440}$, $r = 0.32$	$0.461 + 0.030\tau_{f,440}$, $r = 0.31$	$1.53\tau_{c,440}$	3.34	0.72

ACPD
13, 25013–25065, 2013

Table 4. Refractive index and SSA for biomass burning aerosols from the eight near-source AERONET sites. Note that SSA is calculated for $\tau_{f,550} = 0.5$, $\tau_{c,550} = 0.03$ as in Fig. 4 and will vary for different AOD.

Site	Refractive index (n-*i*k)				SSA			
	440 nm	675 nm	870 nm	1020 nm	440 nm	675 nm	870 nm	1020 nm
Alta Floresta	1.46–0.011i	1.48–0.0094i	1.48–0.0085i	1.47–0.0082i	0.92	0.92	0.92	0.91
Bonanza Creek	1.52–0.0072i	1.53–0.0047i	1.53–0.0040i	1.52–0.0038i	0.95	0.96	0.97	0.97
Cuiaba	1.46–0.016i	1.48–0.014i	1.49-0.013i	1.49–0.012i	0.89	0.89	0.89	0.87
Jabiru	1.43–0.015i	1.45–0.013i	1.47–0.012i	1.47–0.012i	0.90	0.89	0.89	0.88
Mongu	1.50–0.024i	1.51–0.024i	1.52–0.022i	1.52–0.021i	0.87	0.86	0.84	0.81
Mukdahan	1.44–0.014i	1.46–0.014i	1.46–0.013i	1.46–0.013i	0.91	0.90	0.90	0.89
Skukuza	1.44–0.015i	1.47–0.013i	1.47–0.012i	1.47–0.012i	0.90	0.90	0.89	0.87
Yakutsk	1.48–0.0057i	1.49–0.0047i	1.49–0.0041i	1.48–0.0040i	0.96	0.96	0.96	0.96

ACPD
13, 25013–25065, 2013

Table 5. Geographical/sampling information for AERONET coastal/island sites exhibiting cases of transported smoke.

Site	Latitude, degrees	Longitude, degrees	Elevation m.a.s.l.	Number of retrievals	Dates (YYYYMMDD)
Ascension Island	−7.97600	−14.4150	30	19	20030902–06, 20080904, 20080906–07, 20080919, 20080925, 20080928
Bach Long Vy	20.1330	107.733	5	10	20100506, 20100509, 20110209, 20110224, 20110314, 20110418, 20110421, 20110423
Barrow	71.3120	−156.665	0	5	20040703, 20100612
CEILAP Buenos Aires	−34.5670	−58.5000	10	28	20010803, 20010921–22, 20040813–15, 20040827, 20040904, 20060722, 20060824, 20060910, 20060922, 20100821–22, 20110903
COVE	36.9000	−75.7100	37	12	20020706–09
Darwin	−12.4240	130.892	29	20	20071013, 20071016, 20071018–19, 20091011–12, 20091104
Hornsund	77.0010	15.5600	10	6	20060502–03
Inhaca	−26.0410	32.9050	73	33	20000823, 20000831, 20000902–03, 20000905–06, 20000910, 20000914, 20001004–05, 20001007, 20001009–10, 20010820–21, 20010823, 20010829, 20010908, 20010910–11 20010916
La Jolla	32.8700	−117.250	115	7	20031028, 20070804, 20071024–25
Monterey	36.5930	−121.855	50	4	20080627, 20080710, 20080712
Noto	37.3340	137.137	200	5	20030606, 20080422,
San Nicolas	33.2570	−119.487	133	2	20031027
Saturn Island	48.7830	−123.133	200	22	20080630, 20080701–02, 20100802, 20100804, 20100806, 20100816–17
Sevastopol	44.6160	33.5170	80	28	20070809–10, 20070901–03, 20080801, 20100815–18
Singapore	1.29800	103.780	30	10	20090806–07, 20110905-06, 20120924
Trinidad Head	41.0540	−124.151	105	13	20060925–26, 20080709
UCSB	34.4150	−119.845	33	19	20031025–27, 20070817–18, 20071022–23, 20071025–26

ACPD
13, 25013–25065, 2013

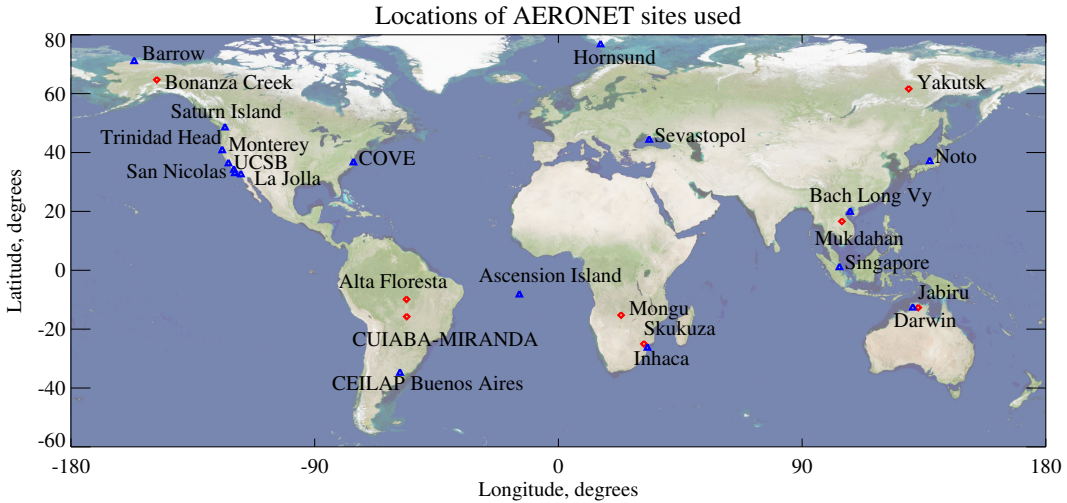

Fig. 1. Locations of AERONET sites used in this work. Red diamonds indicate the near-source sites, and blue triangles the coastal/island sites with occassional cases of transpored smoke-dominated aerosols.

ACPD
13, 25013–25065, 2013

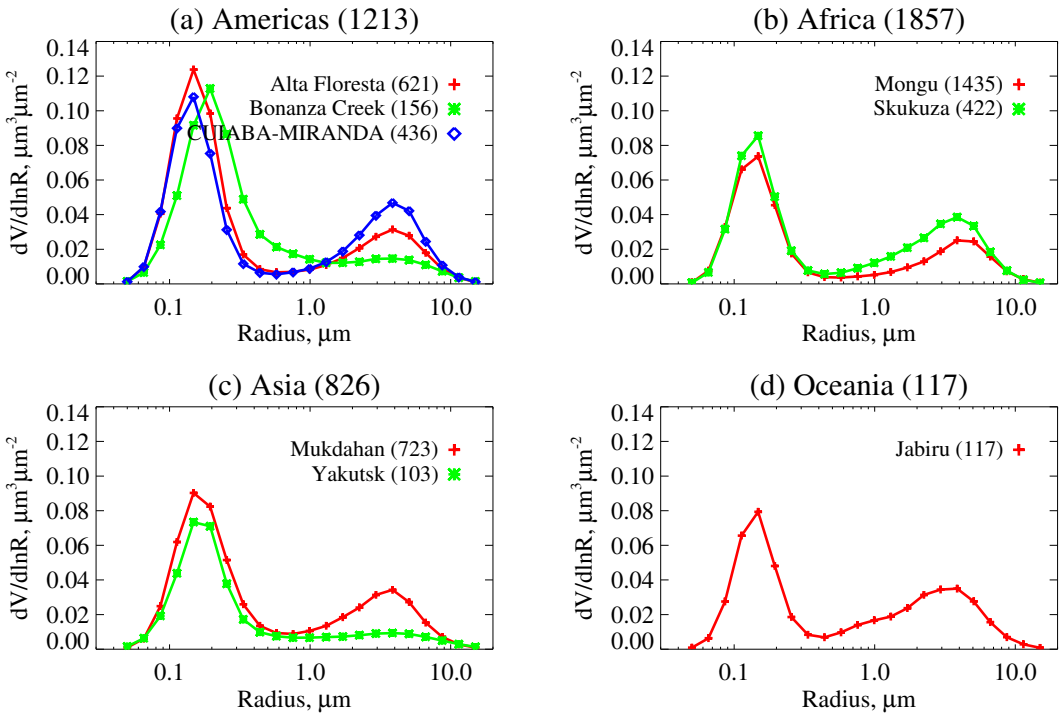

Fig. 2. Median retrieved size distributions from biomass burning cases for near-source AERONET sites considered (Fig. 1, Table 1). Figures in parentheses indicate the number of retrievals for each site/geographical region.

ACPD
13, 25013–25065, 2013

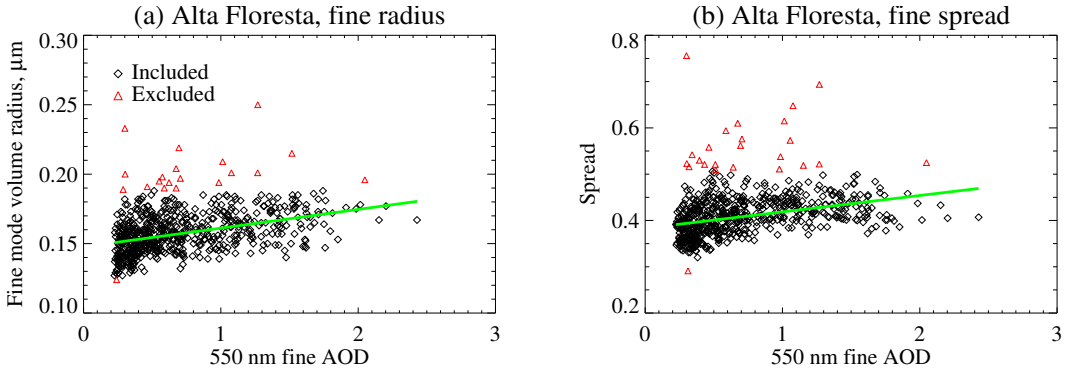

Fig. 3. Example of linear fitting procedure used to arrive at relationships between AOD and fine-mode microphysical model parameters, for Alta Floresta. Black diamonds indicate points used in the fit (green line), while excluded outliers are shown with red triangles. **(a)** shows fine mode volume radius ($r_{v,f}$), and **(b)** the fine mode spread (σ_f).

ACPD
13, 25013–25065, 2013

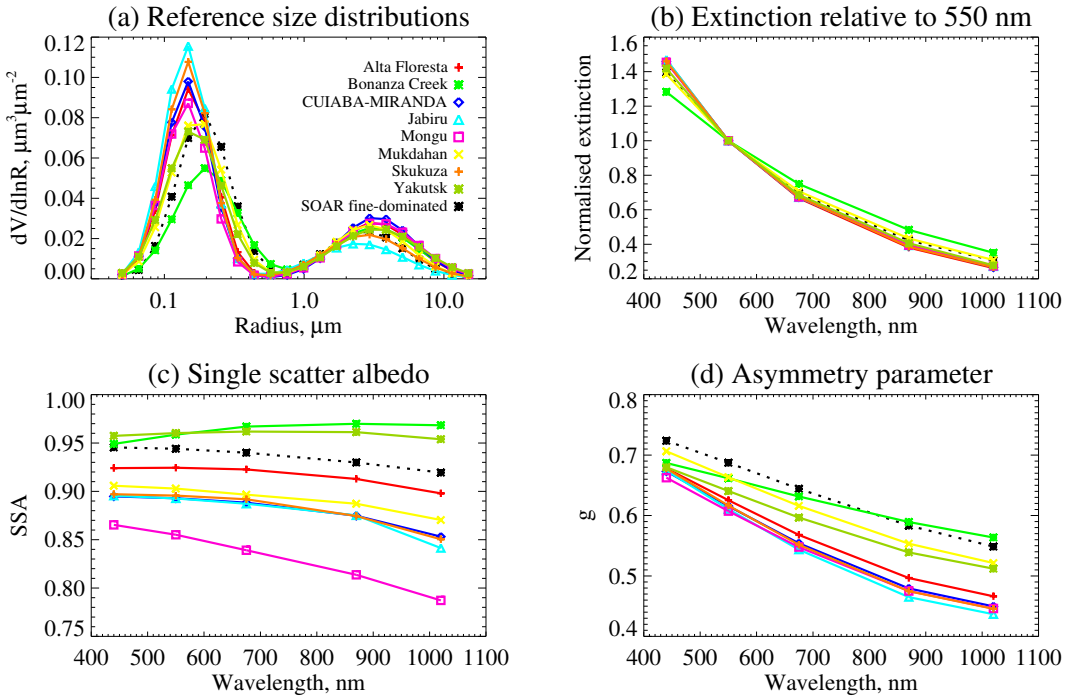

Fig. 4. Properties of smoke aerosols for near-source sites, for a reference fine-mode AOD of 0.5 and coarse-mode AOD of 0.03 at 550 nm. Also shown is the "fine-dominated" model of Sayer et al. (2012a) used in the SeaWiFS Ocean Aerosol Retrieval (SOAR) dataset. Panels show **(a)** size distributions, and spectral **(b)** extinction, **(c)** single scatter albedo, and **(d)** asymmetry parameter.

ACPD
13, 25013–25065, 2013

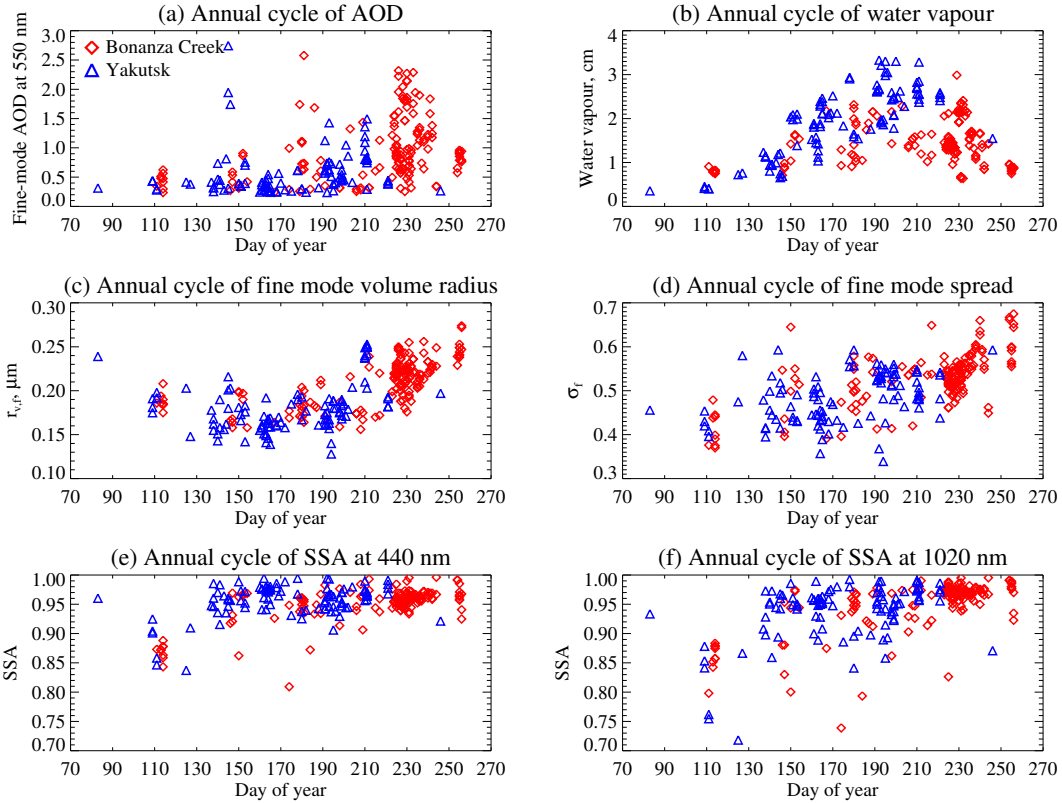

Fig. 5. Annual cycle of AERONET-retrieved aerosol properties and water vapor at Bonanza Creek and Yakutsk. Panels show (a) $\tau_{f,550}$, **(b)** columnar water vapour, **(c, d)** fine mode size, and **(e, f)** aerosol SSA.

ACPD
13, 25013–25065, 2013

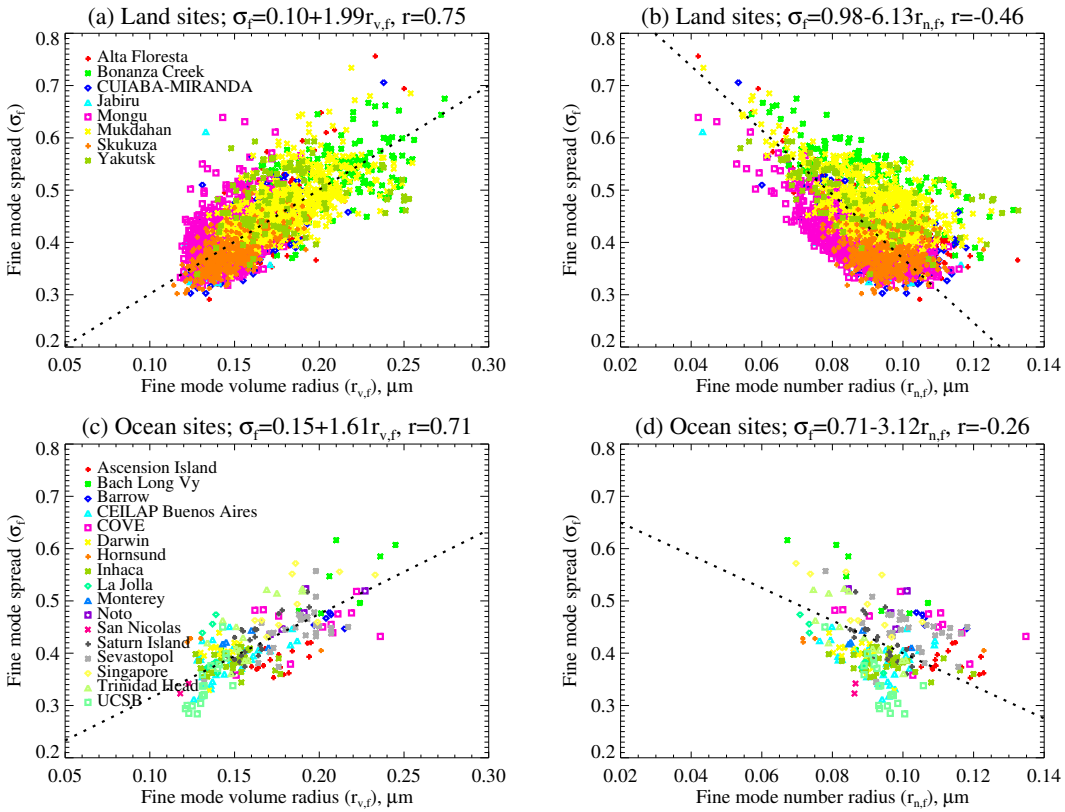

Fig. 6. Linear relationships between fine-mode median radius and spread. **(a, b)** consider near-source land AERONET sites for volume and number radii respectively (legend in **a**), and **(c, d)** coastal/island transported smoke cases for volume and number radii (legend in **c**).

ACPD
13, 25013–25065, 2013

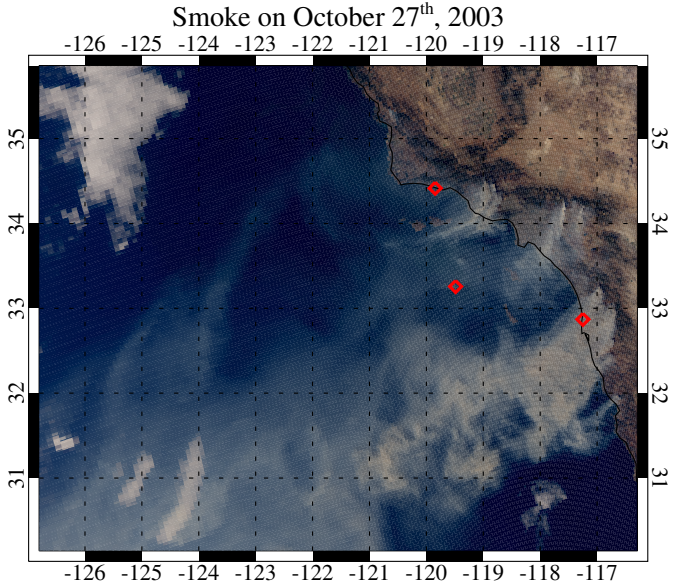

Fig. 7. True-colour image from MODIS aboard the Aqua satellite showing smoke (grey-brown hues) blowing from fires in California (USA) into the Pacific Ocean on 27 October 2003. Red diamonds show, from North to South, the locations of the UCSB (34.4° N, 119.8° W), San Nicolas (33.3° N, 119.5° W), and La Jolla (32.9° N, 117.3° W) AERONET sites.

ACPD
13, 25013–25065, 2013

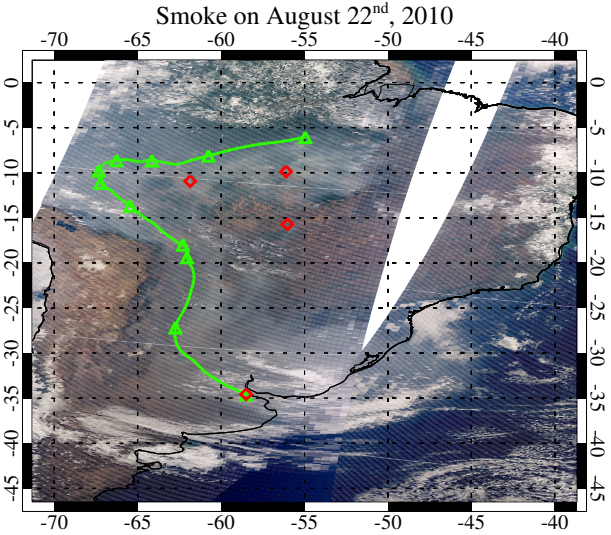

Fig. 8. True-colour image from MODIS aboard the Terra satellite showing smoke (grey-brown hues) spreading across South America and into the southern Atlantic Ocean on 22 August 2010. Image acquired from two consecutive Terra orbits. Red diamonds show, from North to South, the locations of the Alta Floresta (9.87° S, 56.1° W), Ji-Paraná SE (10.9° S, 61.9° W), CUIABA-MIRANDA (15.7° S, 56.1° W), and CEILAP-Buenos Aires (34.6° S, 58.5° W) AERONET sites. The green line shows the HYSPLIT 10-day back-trajectory for the air mass ending at 2 km above Buenos Aires at 00:00 UTC on 23 August 2010; triangles indicate the position at 00:00 UTC each day.

ACPD
13, 25013–25065, 2013

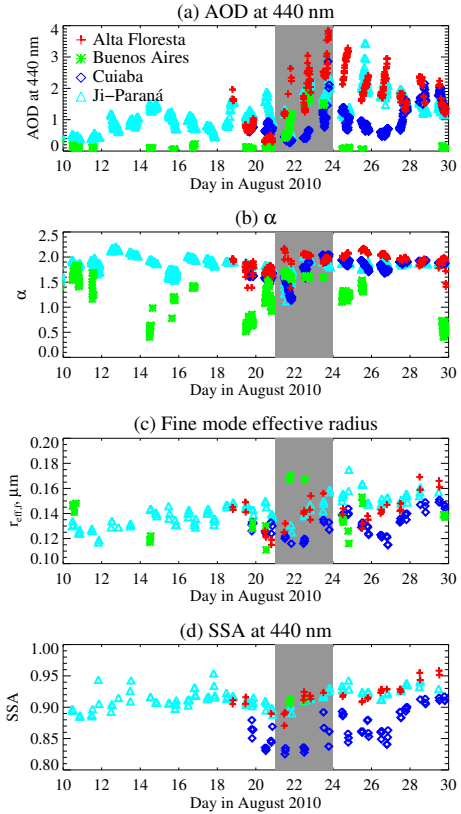

Fig. 9. Time series of aerosol properties at AERONET sites shown in Fig. 8 for 10–30 August 2010. Panels show **(a)** τ_{440}, **(b)** α (both from the direct-Sun AERONET observations), **(c)** $r_{eff,f}$, and **(d)** SSA at 440 nm (both from the AERONET inversion dataset). The shaded grey area indicates 21–23 August when the smoke plume was observed at Buenos Aires.

ACPD
13, 25013–25065, 2013

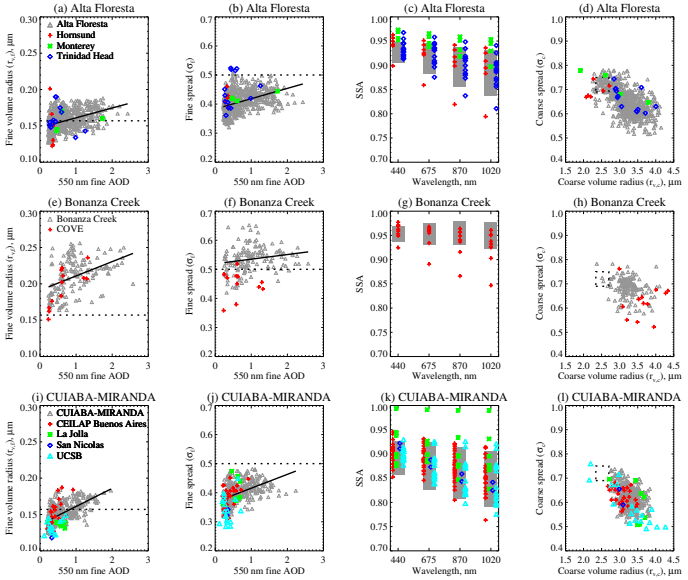

Fig. 10. Properties of smoke-dominated aerosol from near-source sites located in the Americas (Fig. 2), and transported smoke cases for which these sites provide the closest match. From left-right, plots compare fine mode radius, fine mode spread, aerosol SSA (different sites offset slightly for clarity), and coarse mode properties. Grey triangles show the data (with outliers removed, as described in the text) and solid lines the linear fit (Fig. 3). In the SSA plots, the shaded grey area indicates the central 68 % of retrieved values at this site. Dashed lines indicate properties for unpolluted marine aerosol from Sayer et al. (2012b); in the coarse-mode properties plot, the dashed box encloses the range of average radii/spreads for marine aerosol for different wind speed regimes. In all plots, coloured symbols indicate the cases of transported smoke from different sites, as indicated by the legend.

ACPD
13, 25013–25065, 2013

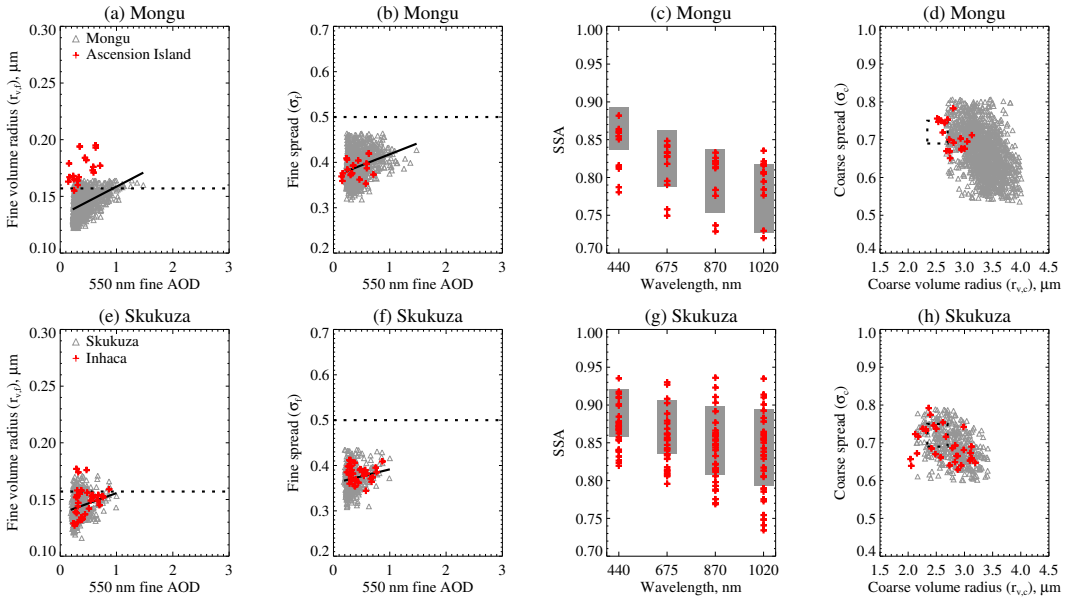

Fig. 11. As Fig. 10, except for near-source sites located in Africa (Fig. 2).

ACPD
13, 25013–25065, 2013

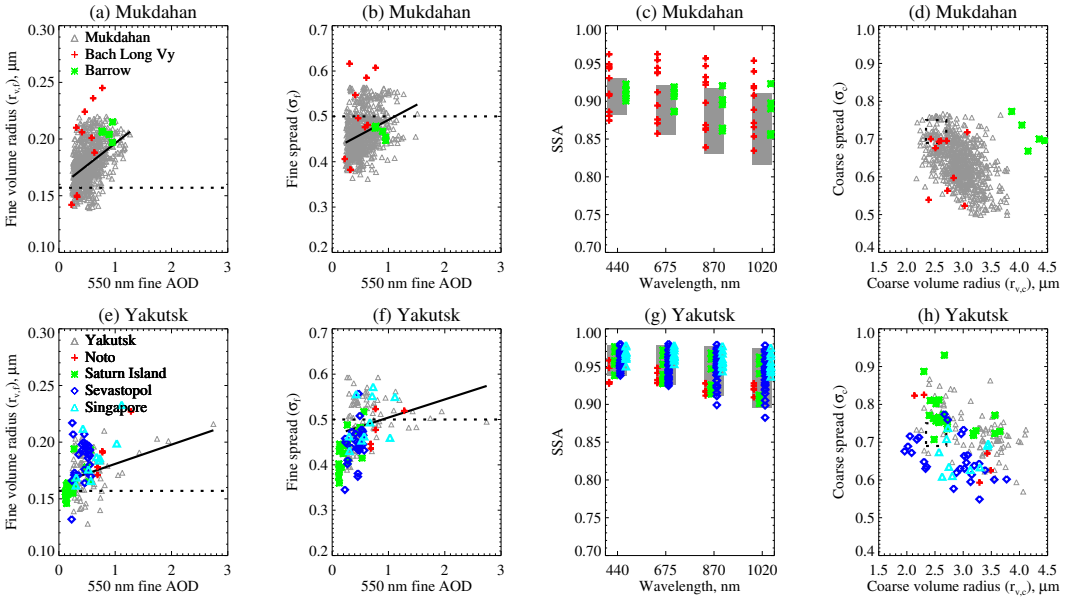

Fig. 12. As Fig. 10, except for near-source sites located in Asia (Fig. 2).

ACPD
13, 25013–25065, 2013

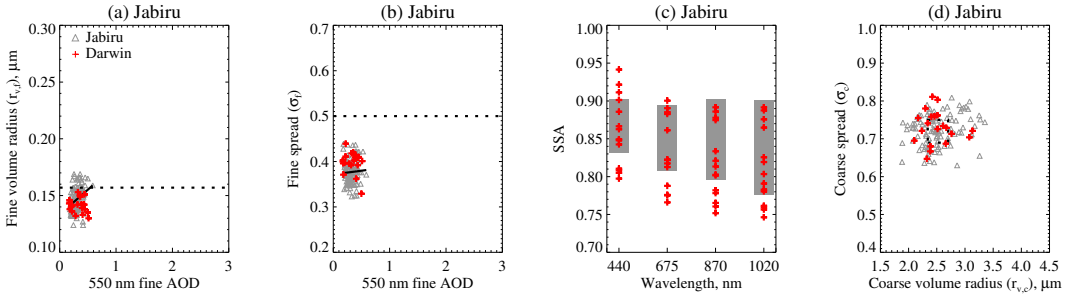

Fig. 13. As Fig. 10, except for near-source sites located in Oceania (Fig. 2).

ACPD
13, 25013–25065, 2013

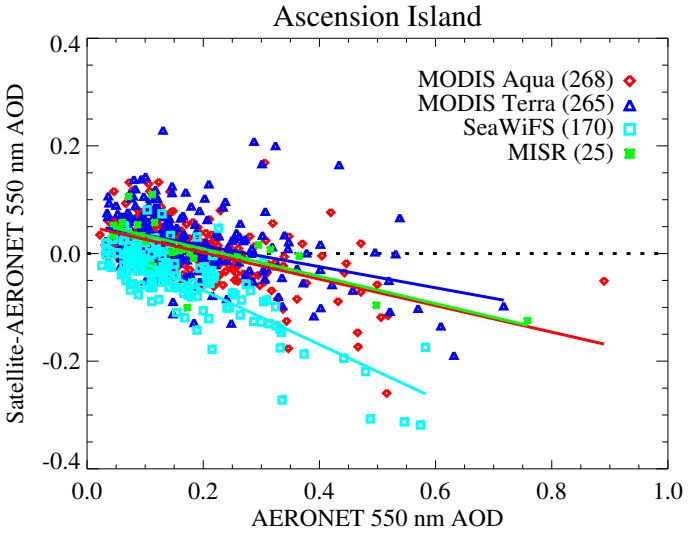

Fig. 14. Error on retrieved AOD at 550 nm as a function of AERONET AOD at 550 nm, from MODIS, SeaWiFS, and MISR data products at Ascension Island. Coloured lines indicate the least-squares linear fit of bias vs. AOD for each dataset. The number of matches for each sensor is shown in parantheses.

ACPD
13, 25013–25065, 2013

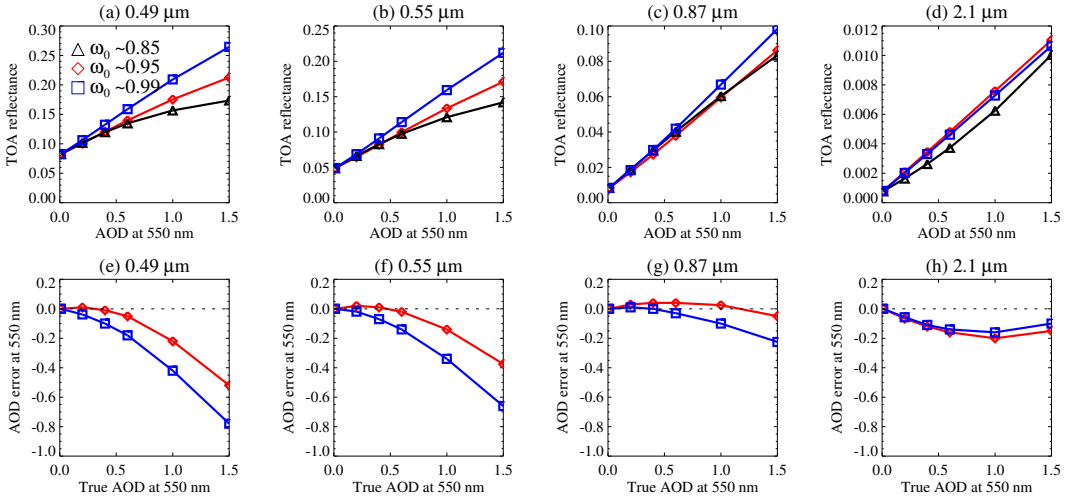

Fig. 15. TOA reflectance and AOD retrieval errors for four wavelengths. **(a–d)** show TOA reflectance as a function of τ_{550}, for strongly (black), moderately (red), and weakly (blue) absorbing aerosol microphysical models over ocean. **(e–f)** show the error in AOD which would be retrieved if measurements at that wavelength were used and a moderately- or weakly-absorbing aerosol assumed, if the true aerosol were instead strongly-absorbing.

ACPD
13, 25013–25065, 2013